iScience

CellPress
OPEN ACCESS

Article

A Unique Energy-Saving Strategy during Hibernation Revealed by Multi-Omics Analysis in the Chinese Alligator

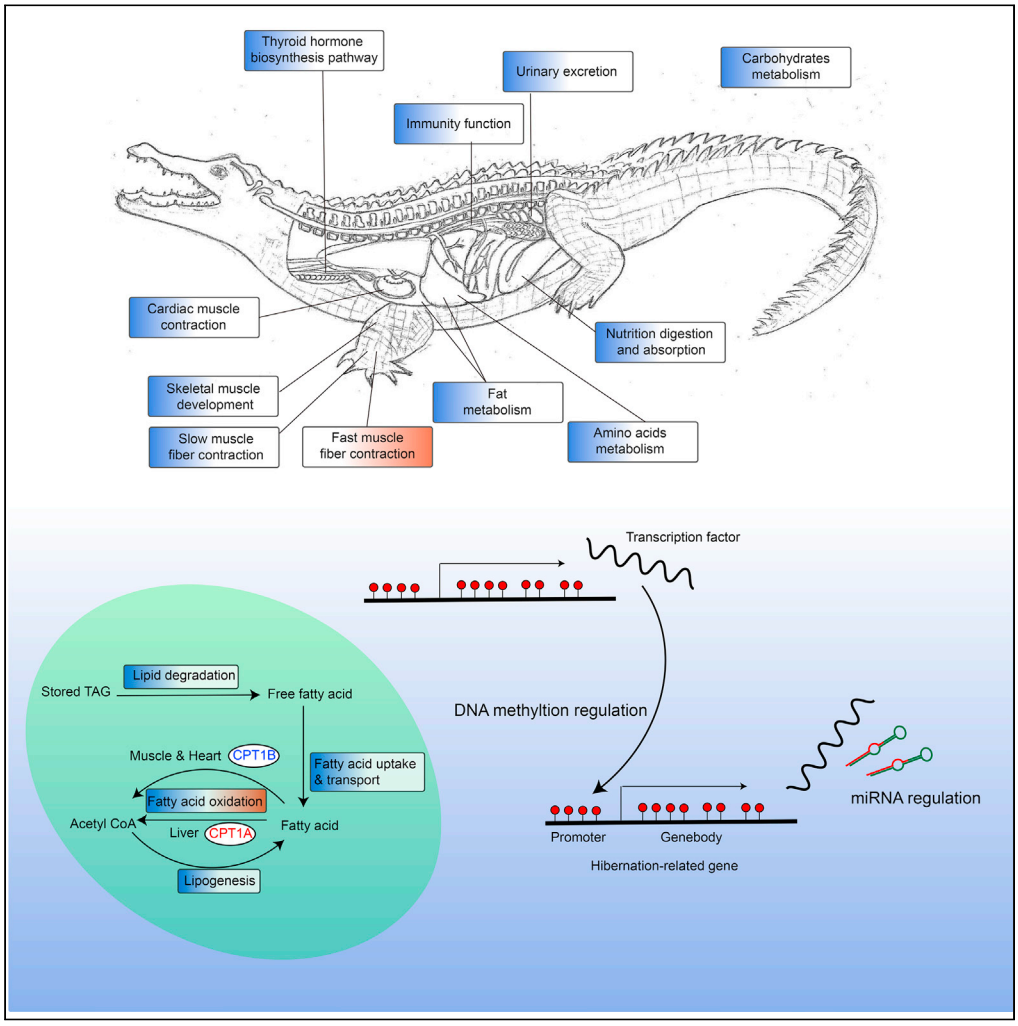

Jian-Qing Lin, Yun-Yi Huang, Meng-Yao Bian, Qiu-Hong Wan, Sheng-Guo Fang

sgfanglab@zju.edu.cn

HIGHLIGHTS

Metabolic and physiological pathways are overall suppressed during hibernation

Suppressed fat catabolism with active *CPT1A* suggests a unique energy-saving strategy

Hibernation-related genes are controlled by methylation-dependent transcription network

miRNAs play complex post-transcriptional regulation roles during hibernation

Lin et al., iScience *23*, 101202
June 26, 2020
https://doi.org/10.1016/j.isci.2020.101202

iScience

CellPress
OPEN ACCESS

Article

A Unique Energy-Saving Strategy during Hibernation Revealed by Multi-Omics Analysis in the Chinese Alligator

Jian-Qing Lin,[1] Yun-Yi Huang,[1] Meng-Yao Bian,[1] Qiu-Hong Wan,[1] and Sheng-Guo Fang[1,2,*]

SUMMARY

Many ectotherms hibernate in face of the harsh winter conditions to improve their survival rate. However, the molecular mechanism underlying this process remains unclear. Here, we explored the hibernation mechanism of Chinese alligator using integrative multi-omics analysis. We revealed that (1) the thyroid hormone biosynthesis, nutrition absorption and metabolism, muscle contraction, urinary excretion and immunity function pathways are overall downregulated during hibernation; (2) the fat catabolism is completely suppressed, contrasting with the upregulation of hepatic fatty-acid-transporter *CPT1A*, suggesting a unique energy-saving strategy that differs from that in hibernating mammals; (3) the hibernation-related genes are not only directly regulated by DNA methylation but also controlled by methylation-dependent transcription networks. In addition, we identified and compared tissue-specific, species-specific, and conserved season-biased miRNAs, demonstrating complex post-transcriptional regulation during hibernation. Our study revealed the genetic and epigenetic mechanisms underlying hibernation in the Chinese alligator and provided molecular insights into the evolution of hibernation regulation.

INTRODUCTION

Many reptiles and amphibians survive winter in refuges where they enter a state of dormancy, which allows them to substantially save energy. This is often referred to as hibernation, although the process itself is very different from that in mammals (Staples, 2016), as the body temperature of ectotherms is cooled to an ambient temperature by the Q10 effect, rather than through blocking thermoregulatory heat production (Grigg and Kirshner, 2015). Nonetheless, akin to mammals, the metabolic rates of hibernating ectotherms are strongly suppressed and their physical states and cardiovascular functions are dramatically altered (Herbert and Jackson, 1985; Storey, 1996) to a level that exceeds the passive effects of cooling, processes that are critical for their long-term survival during hibernation.

The Chinese alligator (*Alligator sinensis*) is a critically endangered freshwater crocodilian endemic to China (Wan et al., 2013) that diverged from the American alligator (*Alligator mississippiensis*) 31–58 million years ago (Oaks, 2011). Both species of the *Alligator* genus live at higher, thus cooler, latitudes than other crocodilian species and enter hibernation so as to survive the cold winter (Chen et al., 2003; Grigg and Kirshner, 2015). Typically, the Chinese alligator stops eating and goes into hibernation when temperatures drop in late October until late March (Chen et al., 2003; Fang et al., 2015). During this time, their metabolism is strongly suppressed and the animals sleep continuously unless they are disturbed (Fang et al., 2015). The quality of this hibernation period (as defined by undisturbed sleep in a temperature-appropriate environment) is known to exert a crucial impact on their health (Chen et al., 2003; Xia et al., 2006; Zhang et al., 2003). In addition to human hunting and habitat disruption, global climate change is becoming a critical threat to Chinese alligators, as indeed it is for many other hibernators (Humphries et al., 2002; Inouye et al., 2000). Therefore, exploring the gene regulatory network underlying seasonal physiological changes is not only important for revealing how hibernating ectotherms overcome the cold and foodless winter in their habitat but may also ultimately aid their conservation in the future.

Various studies over the past half century have investigated the molecular mechanisms underlying hibernation, and numerous associated genes and pathways have been identified (Storey, 2006; Storey and

[1]MOE Key Laboratory of Biosystems Homeostasis & Protection, State Conservation Centre for Gene Resources of Endangered Wildlife, College of Life Sciences, Zhejiang University, Hangzhou 310058, P. R. China

[2]Lead Contact

*Correspondence: sgfanglab@zju.edu.cn

https://doi.org/10.1016/j.isci.2020.101202

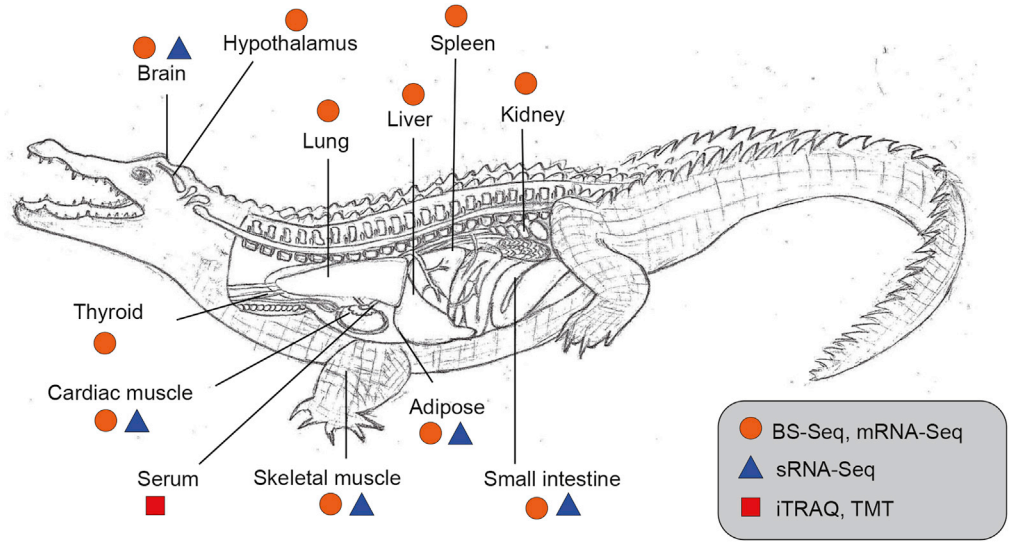

Figure 1. Chinese Alligator Tissue Samples Used in this Study
See also Table S1.

Storey, 2007, 2013). With the development of high-throughput sequencing, mRNA-sequencing (mRNA-seq) has been used to explore the molecular and genetic bases of hibernation. However, these studies generally focused on mammalian hibernators (Cooper et al., 2016; Faherty et al., 2016, 2018; Hampton et al., 2013; Lei et al., 2014; Luan et al., 2018; Nespolo et al., 2018), with only a few studies in reptiles (Capraro et al., 2019; Sun et al., 2018). As the two transcriptome studies in reptile hibernators focused on only three tissues (heart, skeletal muscle, and kidneys/brain), there is a clear interest in characterizing genome-wide regulatory networks underlying hibernation in the Chinese alligator using more tissues, especially those in charge of metabolism.

Epigenetic mechanisms mediate gene-environment interactions in various biological processes. DNA methylation is an ancient epigenetic modification in eukaryotic genomes that plays essential roles in various biological processes, including the regulation of gene expression, development, and stress responses (Breiling and Lyko, 2015; Pelizzola and Ecker, 2011; Smith and Meissner, 2013; Su et al., 2011). The level and pattern of DNA methylation typically varies among species and cell types. Usually, promoter methylation is negatively correlated with gene transcription levels, whereas methylation in the gene body is associated with active transcription (Jones, 2012). DNA methylation reportedly plays an important role in the regulation of gene expression associated with mammal hibernation (Alvarado et al., 2015; Biggar and Storey, 2014b; Fujii et al., 2006); however, previous studies largely focused on changes in overall DNA methylation levels, or methylation of specific genes. MicroRNAs (miRNAs) are another epigenetic mechanism involved in hibernation (Arfat et al., 2018; Biggar and Storey, 2015; Lyons et al., 2013). DNA methylation is associated with gene transcription potential, whereas miRNAs participate in post-transcriptional regulation. Although animal miRNAs are phylogenetically conserved (Ambros, 2004), seasonal expression changes vary among species and even tissues (Arfat et al., 2018; Biggar and Storey, 2015; Lyons et al., 2013).

We collected tissues and serum samples from adult Chinese alligators in winter (the coldest time of the year in the Chinese alligator habitat) and summer (the active season of the Chinese alligator) and analyzed them using mRNA-seq, bisulfite sequencing (BS-seq), small RNA sequencing (sRNA-seq), and iTRAQ/TMT protein analysis to comprehensively explore the genetic and epigenetic mechanisms underlying reptile hibernation (Figure 1, Table S1, Supplementary Text).

RESULTS

Energy Metabolism Is Suppressed during Hibernation

To gain insights into the molecular mechanisms that enable the Chinese alligator to substantially save energy during hibernation, we compared the transcriptomes of tissues and proteomes of serum collected

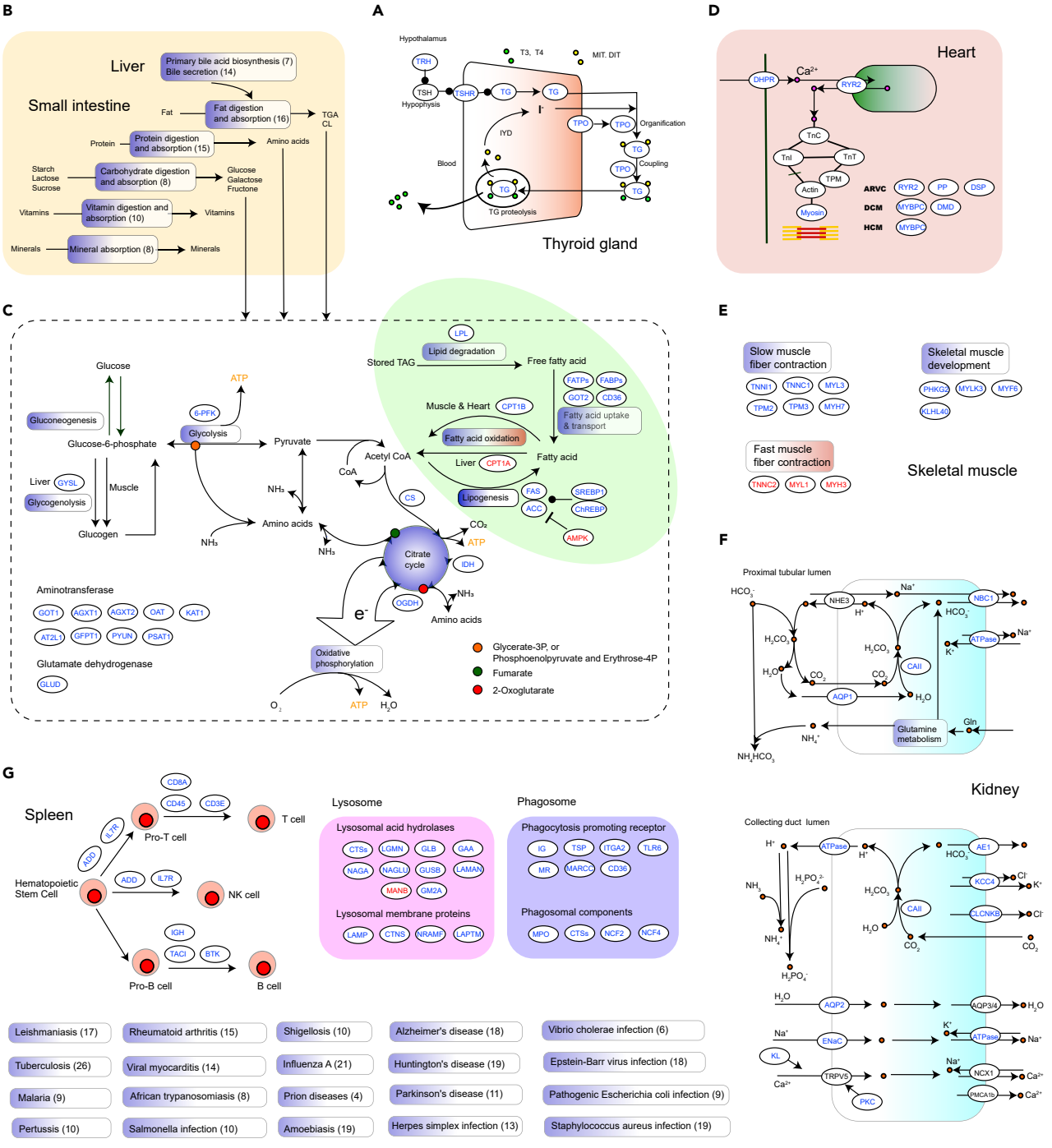
B
Liver
Primary bile acid biosynthesis (7)
Bile secretion (14)
Small intestine
Fat
Fat digestion and absorption (16)
TGA CL
Protein
Protein digestion and absorption (15)
Amino acids
Starch Lactose Sucrose
Carbohydrate digestion and absorption (8)
Glucose Galactose Fructone
Vitamins
Vitamin digestion and absorption (10)
Vitamins
Minerals
Mineral absorption (8)
Minerals
A
Hypothalamus
TRH
T3, T4
MIT, DIT
TSH
Hypophysis
TSHR
TG
I-
IYD
Blood
TPO
Organification
Coupling
TG proteolysis
Thyroid gland
D
Heart
DHPR
Ca2+
RYR2
TnC
TnI
TnT
TPM
Actin
Myosin
ARVC
DCM
HCM
RYR2
PP
DSP
MYBPC
DMD
MYBPC
C
Glucose
ATP
Gluconeogenesis
6-PFK
Glycolysis
Glucose-6-phosphate
Pyruvate
Liver
GYSL
Muscle
Glycogenolysis
Glucogen
NH3
Amino acids
CoA
Acetyl CoA
CS
Citrate cycle
CO2
ATP
IDH
NH3
OGDH
Amino acids
e-
Oxidative phosphorylation
O2
ATP
H2O
LPL
Lipid degradation
Stored TAG
Free fatty acid
FATPs
FABPs
GOT2
CD36
Muscle & Heart
CPT1B
Fatty acid uptake & transport
Fatty acid oxidation
Liver
CPT1A
Fatty acid
Lipogenesis
FAS
ACC
SREBP1
ChREBP
AMPK
Aminotransferase
GOT1
AGXT1
AGXT2
OAT
KAT1
AT2L1
GFPT1
PYUN
PSAT1
Glutamate dehydrogenase
GLUD
Glycerate-3P, or Phosphoenolpyruvate and Erythrose-4P
Fumarate
2-Oxoglutarate
E
Slow muscle fiber contraction
TNNI1
TNNC1
MYL3
TPM2
TPM3
MYH7
Fast muscle fiber contraction
TNNC2
MYL1
MYH3
Skeletal muscle development
PHKG2
MYLK3
MYF6
KLHL40
Skeletal muscle
F
Proximal tubular lumen
HCO3-
NHE3
Na+
H+
NBC1
H2CO3
H2O
CO2
CAII
AQP1
ATPase
K+
Glutamine metabolism
Gln
NH4+
NH4HCO3
Kidney
Collecting duct lumen
AE1
KCC4
Cl-
K+
CLCNKB
NH3
H2PO2-
H2PO4-
AQP2
AQP3/4
ENaC
KL
TRPV5
PKC
NCX1
PMCA1b
Ca2+
G
Spleen
CD8A
CD45
CD3E
T cell
Pro-T cell
IL7R
ADD
Hematopoietic Stem Cell
NK cell
IGH
TACI
BTK
Pro-B cell
B cell
Lysosome
Lysosomal acid hydrolases
CTSs
LGMN
GLB
GAA
NAGA
NAGLU
GUSB
LAMAN
MANB
GM2A
Lysosomal membrane proteins
LAMP
CTNS
NRAMP
LAPTM
Phagosome
Phagocytosis promoting receptor
IG
TSP
ITGA2
TLR6
MR
MARCO
CD36
Phagosomal components
MPO
CTSs
NCF2
NCF4
Leishmaniasis (17)
Tuberculosis (26)
Malaria (9)
Pertussis (10)
Rheumatoid arthritis (15)
Viral myocarditis (14)
African trypanosomiasis (8)
Salmonella infection (10)
Shigellosis (10)
Influenza A (21)
Prion diseases (4)
Amoebiasis (19)
Alzheimer's disease (18)
Huntington's disease (19)
Parkinson's disease (11)
Herpes simplex infection (13)
Vibrio cholerae infection (6)
Epstein-Barr virus infection (18)
Pathogenic Escherichia coli infection (9)
Staphylococcus aureus infection (19)
Graphic example
MYH3
Upregulated DEG during hibernation
KAT1
Downregulated DEG during hibernation
Fast muscle fiber contraction
Upregulated pathway during hibernation
Gluconeogenesis
Downregulated pathway during hibernation
Fatty acid oxidation
Pathway show different changes in different tissues
Leishmaniasis (17)
Number in bracket: the number of downregulated DEGs in the pathway
Activate or upregualted of transcription
Inactivate or downregualted of transcription
Direction of reaction or transfer

Figure 2. Changes in Gene Expression in Pathways Participating in Energy Metabolism in Multiple Tissues during Hibernation in the Chinese Alligator

(A)Thyroid hormone synthesis pathway in the thyroid gland.

(B) Pathways involved in nutrient digestion and absorption in the liver and small intestine in the female alligator and corresponding numbers of winter-repressed DEGs (numbers in the brackets).

(C) Gene expression patterns in pathways participating in lipid metabolism (highlighted by green background), carbohydrate metabolism, and amino acid metabolism.

(D) DEGs involved in cardiac contraction and heart disease.

(E) DEGs involved in skeletal muscle contraction and development.

(F) Gene expression pattern in the pathways participating in renal function.

(G) Pathways involved in immunity and disease in the spleen.

See also Figures S1–S3 and Tables S2, S3, and S4.

during winter and summer periods. The seasonal transcriptome variations were matched to the biological functions of different tissues. In order to correlate this with the BS-seq and sRNA-seq data, we focused on the transcriptomes of the female alligator in most of the subsequent analyses. However, we note that gene expression patterns were largely similar in tissues from male and female animals.

Thyroid Hormone Biosynthesis and Signaling

The hypothalamus-pituitary-thyroid axis is essential for metabolism regulation. Our results revealed that both the thyrotropin-releasing hormone gene (*TRH*) in the hypothalamus and the thyroid hormone biosynthesis pathway in the thyroid glands are downregulated during hibernation. KEGG pathway analysis revealed that the "thyroid hormone biosynthesis pathway" was enriched in downregulated differentially expressed genes (DEGs) during hibernation (winter-suppressed DEGs) in the thyroid gland ($q < 0.05$) (Table S2). Various genes involved in thyroid hormone biosynthesis, including *TSHR*, *TG*, and *TPO*, are suppressed in winter (Figure 2A). Correspondingly, serum levels of thyroid hormones (T3, T4, free T3, and free T4), TG antibody, and TPO antibody are substantially lower in winter (Table S3). iTRAQ/TMT analysis of serum samples indicated that von Willebrand factor (VWF), cartilage oligomeric matrix protein (COMP), and actin 5 (ACT5) in the "thyroid hormone signaling pathway" are significantly downregulated in winter (Table S4). We assumed that fuel use and physiological states would be altered significantly during hibernation (see below) owing to the downregulation of the thyroid hormone.

Digestion and Absorption

Food digestion and absorption largely take place in the small intestine, and fat is digested with the aid of bile acid synthesized by the liver. KEGG pathway analysis revealed that "primary bile acid biosynthesis" (liver), "fat digestion and absorption," "vitamin digestion and absorption," and "mineral absorption" (small intestine) were significantly enriched ($q < 0.05$) in winter-suppressed DEGs (Figures 2B and S1A, Table S2). Significantly more downregulated than upregulated DEGs (Wilcoxon signed-rank test, $q < 0.05$) were observed in digestion- and absorption-related pathways (Figure S1). These results suggested that digestion and absorption in the small intestine and bile acid biosynthesis and secretion in the liver are suppressed during hibernation, which is consistent with the alligator's fasting state in winter.

Nutrient Metabolism

Carbohydrates are the primary energy source in animals and are degraded for ATP production through glycolysis/gluconeogenesis, the citrate cycle (tricarboxylic acid cycle), and oxidative phosphorylation. Significantly more winter-suppressed than winter-activated DEGs (Wilcoxon signed-rank test, $q < 0.05$) were observed in these three pathways (Figures 2C and S2A). Particularly, genes encoding rate-limiting enzymes of glycolysis (*6-PFK*) and the citrate cycle (*CS*, *IDH*, and *OGDH*) were significantly downregulated during hibernation in most tissues (Figure 2C). Pyruvate kinase genes (*KPM* and *KPLR*) showed limited seasonal differences in most tissues, whereas KPM and KPLR proteins in the serum were significantly downregulated during hibernation (Table S3), suggesting post-transcriptional regulation of these two factors. Glycogen serves as a form of energy storage mainly in the liver and muscles. Glycogen serves as a form of energy storage, mainly in the liver and muscles. The expression of the liver glycogen synthase gene *GYSL*, but not that of the muscle glycogen synthase gene *GYSM* or glycogen phosphorylase genes (*GYPL*, *GYPM*, and *GYPB*), was significantly downregulated during hibernation (Figure 2C). Conversely, the expression of the muscle glycogen phosphorylase gene *GYPM* was considerably upregulated, although not statistically significantly ($q = 6.85 \times 10^{-36}$, fold change = 1.48). These results suggested

that fasting during hibernation leads to suppression of carbohydrate catabolism and hepatic glycogen synthesis, but stored glycogen may be, at least partly, a reserve energy source.

Fat is another form of energy storage. Unlike mammals, the fat catabolism pathway was not upregulated during hibernation; instead, the expression of lipid metabolic pathway genes was generally downregulated in the hibernating Chinese alligator. In adipose and liver tissues of female alligators, the "PPAR signaling pathway," which is involved in lipid metabolism regulation, was significantly enriched ($q < 0.05$) in case of DEGs suppressed during the winter (Table S2). Lipoprotein lipase (LPL) hydrolyzes triacylglycerols in chylomicrons in adipose tissue, the heart, and skeletal muscle into fatty acid (FA) and glycerin, whereas hormone-sensitive lipase (HSL) hydrolyzes dietary fat. During hibernation, *LPL* expression was suppressed in adipose tissue, the heart, and skeletal muscle, whereas *HSL* expression was not significantly changed (Figures 2C and S2B). Genes involved in fatty acid transport and uptake, including the *FATP* family, *FABP* family, *GOT2*, and *CD36*, were also downregulated in winter (Figures 2C and S2B). FA oxidation is regulated by the rate-limiting enzymes CPT1A (liver) and CPT1B (heart and skeletal muscle) (Britton et al., 1997). During hibernation, *CPT1A2* was upregulated, whereas *CPT1B* was downregulated (Figures 2C and S2B). These results suggested that, although utilization of stored fat decreased during hibernation, the Chinese alligator makes greater use of FAs in the liver to maintain its normal function and metabolic activity but saves energy by using less fat in the heart and skeletal muscle. This is a unique energy-saving strategy different from that in hibernating mammals, which extensively upregulate fat catabolism-related genes and fully utilize fat. Fatty acid biosynthesis takes place mainly in the liver. The KEGG pathways "biosynthesis of unsaturated fatty acids" and "fatty acid biosynthesis" were significantly enriched ($q < 0.05$) in winter-suppressed DEGs in the livers of female alligators (Table S2). In particular, key genes *ACC* and *FAS*, and their enhancing factors *SREBP1* and *ChREBP*, were significantly downregulated, whereas *ACC* inhibitor *AMPK* was upregulated during hibernation (Figures 2C and S2B). This is an energy-saving strategy in the fasting alligator.

Amino acids are metabolized mainly in the liver. Amino acid metabolic genes were generally downregulated in the hibernating alligator. There were substantially more winter-suppressed than winter-activated DEGs in the amino acid metabolism pathways (Wilcoxon signed rank test, $q < 0.05$) (Figure S2C). Winter-suppressed DEGs were enriched for "glycine, serine, and threonine metabolism," "tryptophan metabolism," and "cysteine and methionine metabolism" (Table S2) and included aminotransferase genes (*GOT1*, *AGXT1*, *AGXT2*, *OAT*, *KAT1*, *AT2L1*, *GFPT1*, *PYUN*, and *PSAT1*) and a glutamate dehydrogenase gene (*GLUD*) (Figures 2C and S2D). These results suggested that amino acid metabolism is suppressed during hibernation.

Cardiac Muscle and Skeletal Muscle Contraction

During hibernation, the heart beats slower. Cardiac muscle contraction is a complex process initiated by Ca^{2+} influx. Seven voltage-dependent calcium channel genes (*CACNA1C-1*, *CACNA1C-2*, *CACNA2D2-1*, *CACNA2D2-2*, *CACNA2D1*, *CACNB4*, and *CACNG2*) were downregulated in the hibernating alligator (Figures 2D and S3A). Interestingly, six pathogenicity genes involved in heart failure, i.e., *RYR2*, *DSP*, and *PKP2* for arrhythmogenic right-ventricular cardiomyopathy, *DMD* and *MYBPC3* for dilated cardiomyopathy, and *MYBPC3* for hypertrophic cardiomyopathy, were suppressed during hibernation (Figures 2D and S3A). The downregulation of genes involved in cardiac muscle contraction provides a molecular mechanism underlying the alligator's low heart rate during hibernation.

We also identified various season-biased DEGs involved in skeletal muscle function and development. *PHKG2*, *MYLK3*, *KLHL40*, and *MYF6*, involved in skeletal muscle development, were downregulated during hibernation (Figures 2E and S3B). *TNNI1*, *TNNC1*, *TPM2*, *TPM3*, *MYL3*, and *MYH7*, encoding slow-twitch skeletal muscle components, were also suppressed, whereas *TNNC2*, *MYL1*, and *MYH3*, encoding fast-twitch skeletal muscle components, were upregulated during hibernation (Figures 2E and S3B). These gene expression patterns are consistent with our previous finding that alligators show self-defense behavior when they are disturbed and awakened from hibernation but soon calm down and fall asleep again (Fang et al., 2015).

Urinary Excretion

With the significant decrease in metabolic gene expression, renal function-related gene expression was also expected to be suppressed during hibernation. Indeed, the KEGG pathways "collecting duct acid secretion" and "proximal tubule bicarbonate reclamation" were significantly enriched ($q < 0.05$) in

winter-suppressed DEGs in the kidneys (Table S2). These DEGs included genes encoding CA2, which catalyzes the reversible hydration of carbon dioxide; SNAT3, GLS, and GLUD, which transport and catalyze glutamine to produce NH^{4+}; and many transmembrane transporters in proximal tubular cells (NBC1, ATP1, ATP1B, and AQP1) and collecting duct intercalated cells (AE1, KCC4, CLCNKB, and seven ATPases), which transport ions across urine, cytoplasm, and blood. Various genes involved in the reabsorption of water, calcium, and sodium were downregulated, including AQP2 and ENACA, ENACB and ENACG, as well as VDR, PTHR, and KL, the protein products of which regulate Ca^{2+} channel expression and apical abundance (Figures 2F and S3C). These results indicated that kidney function is suppressed in the hibernating alligator.

Immunity

The spleen is the largest immune organ and is a reservoir of macrophages and lymphocytes, which act as scavengers and in immune defense against pathogens, respectively. Winter-suppressed DEGs in the spleen were enriched in KEGG pathways involved in immunity and hematopoiesis (Table S2). In particular, the downregulated DEGs included genes crucial for lymphocyte production, including *ADD*, *IL7R* (NK-cell and pro-T-cell production), *CD3E*, *CD45*, *CD8A* (T cell production), *IGH*, *BTK*, and *TACI* (B-cell production) (Figure 2G), suggesting that lymphocyte proliferation is suppressed during hibernation. Various genes encoding lysosomal acid hydrolases and lysosomal membrane proteins were significantly downregulated. Genes encoding phagosomal components, including *MPO*, *NCF2*, *NCF4*, and *CTL*, were downregulated, indicating that phagocytosis is suppressed during hibernation (Figure 2G). In addition, various winter-suppressed DEGs are involved in infectious diseases (leishmaniasis, malaria, asthma, tuberculosis, pathogenic *Escherichia coli* infection, etc.) (Figure 2G, Table S2). These results suggested that, as the hibernating Chinese alligator stays in a refuge, where less exogenous pathogens are present, immunity and hemopoiesis are suppressed to save energy.

Factors Actively Upregulated during Hibernation

Several factors actively upregulated during hibernation were identified in the Chinese alligator. The expression of cold-inducible RNA-binding protein genes (*CIRBP*) can be induced simply by cold stress (Saito et al., 2000; Sugimoto and Jiang, 2008). In nearly all tissues, the transcription of *CIRBP* was actively upregulated, especially in the brain, thyroid, liver, small intestine, adipose tissues, kidneys, heart, and skeletal muscle (Figure S3D). These results suggested that *CIRBP* plays a critical, although not fully elucidated, role in the ectotherm hibernator. Unexpectedly, *c-FOS*, a neural activity marker gene (Mateju et al., 2009), was also overexpressed during hibernation in most central and peripheral organs, except the thyroid gland (Figure S3E), suggesting active neural states in the hibernating alligator and its positive regulation during hibernation. Furthermore, general transcription factor (*GTF*) genes were generally activated during winter (Wilcoxon signed-rank test, q = 7.896E-005) (Figure S3F). Thus, the downregulation of genes participating in thyroid hormone biosynthesis, nutrient absorption and metabolism, urinary excretion, and immunity during hibernation is likely not simply regulated via GTF gene repression but by more specific and complex pathways, such as DNA methylation and miRNAs.

DNA Methylation Landscapes in the Hibernating Chinese Alligator

An average of 24.43 M methylated cytosines (mCs) were identified by BS-seq in each tissue sample, accounting for 2.49% of cytosines (Cs) in the Chinese alligator. Most mCs (96.66%) were in CpG context (Figure 3A), whereas mCs in CHG and CHH contexts were rare and were substantially less methylated (Figures 3A and 3B), consistent with findings in other vertebrates (Figure 3C). Therefore, we focused on CpG sites in most of the subsequent analyses.

DNA methylation patterns varied among genome regions. In transcribed regions and ~2 kb upstream and downstream of these regions, CG methylation levels were lowest in the promoter, where the methylation level gradually declined to a minimum at the transcription start site (TSS) and then increased again in the 5′ UTR. CG methylation levels were highest in the exon and intron regions but slightly decreased in the 3′ UTR (Figure 3D). These results suggested that DNA methylation may participate in the regulation of transcription initiation. We also evaluated methylation levels in GC islands, microsatellites, transposable elements, and their adjacent regions. The relatively higher CG methylation levels within transposable elements suggested suppression of active transposons (Figure 3E). No significant difference was found in global DNA methylation patterns between winter and summer samples in terms of methylation broadness and

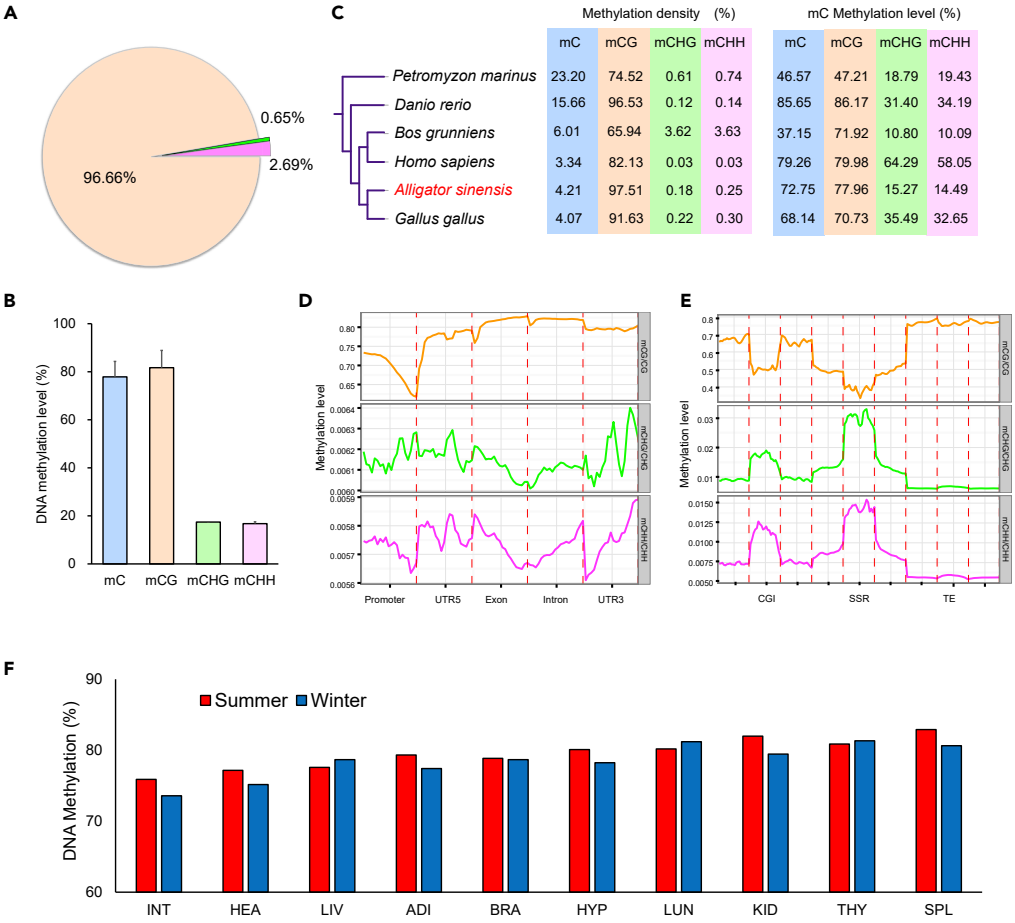

Figure 3. DNA Methylation Patterns in the Hibernating Chinese Alligator

(A) Percentage of methylated cytosines (mC) identified in each sequence context

(B) Average mC level in each indicated sequence context.

(C) mC densities and levels in six chordate species.

(D) DNA methylation levels in different gene features in the Chinese alligator. Promoters encompass 2 kb upstream of the transcription start site.

(E) DNA methylation levels in CG island (CGI), simple-sequence repeat (SSR), and transposable element (TE) regions and 2 kb upstream and downstream.

(F) DNA methylation level in the CG context of each tissue in inactive (winter) and active (summer) periods.

See also Figure S4.

deepness levels ($p > 0.05$), suggesting that the regulation of DNA methylation in hibernation is not simply through overall hyper- or hypomethylation (Figure 3F, Figure S4).

Correlation between DNA Methylation Status and Gene Expression

To explore potential regulatory roles of DNA methylation in gene expression in the hibernating Chinese alligator, we correlated mRNA-seq data with BS-seq data obtained from the same tissues. Promoter CG methylation was negatively correlated with gene expression. As for CG methylation in the gene body and downstream thereof, non-expressed genes had the lowest DNA methylation levels, whereas genes with intermediate expression demonstrated the highest DNA methylation levels (Figure 4A). Genes with the highest gene-body methylation levels (fourth and fifth groups in Figure 4B) tended to be expressed at intermediate levels. These results suggested that promoter hypermethylation is associated with transcriptional repression, whereas gene-body methylation plays a role in the normalization of gene overexpression.

To explore DNA methylome alterations in the hibernating Chinese alligator, we identified differentially methylated genes (DMGs) between winter and summer samples. DEGs were significantly enriched among

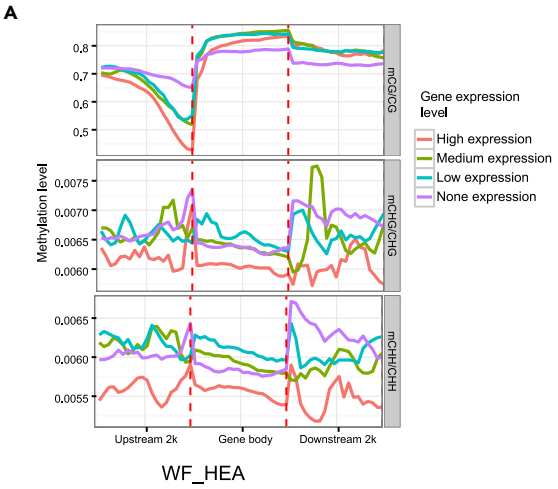

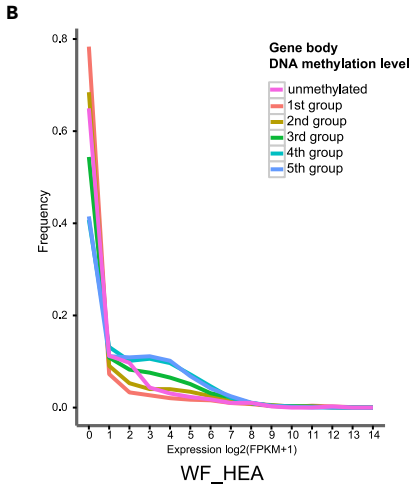

C

	DEG	DMG	DEG with DMR	Obs/Exp	Fisher's exact test
ADI	2174	1285	162	1.599	5.325E-09
LIV	2344	840	147	2.059	1.303E-16
MUS	1125	280	30	2.626	2.190E-06
HEA	1647	1157	102	1.476	8.524E-07
INT	2118	288	33	1.492	2.200E-02
SPL	2505	514	94	2.013	3.786E-11
BRA	2692	1534	244	1.629	8.825E-10
LUN	3620	821	177	1.642	1.734E-11
KID	1907	319	31	1.405	5.394E-02
HYP	1305	424	34	1.694	8.150E-03
THY	1721	292	41	2.250	1.483E-07

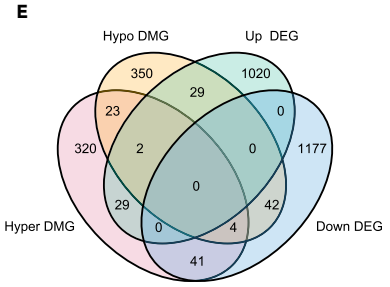

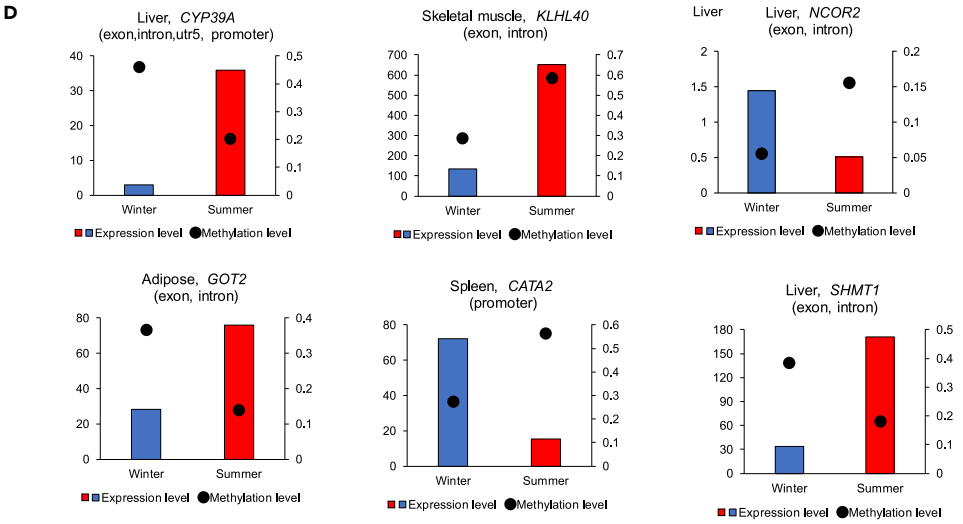

Figure 4. DNA Methylation Regulation of Gene Expression during Chinese Alligator Hibernation

(A) Distributions of methylation levels within gene bodies and 2-kb upstream and downstream regions by different expression levels. Based on the expression level, protein-coding genes were divided into two groups: non-expressed genes (FPKM <1) and expressed genes. The latter were further divided into three groups: low-expression genes (FPKM < lower quartile), intermediate-expression genes (upper quartile < FPKM < upper quartile), and high-expression genes (FPKM > upper quartile).

(B) Expression profiles of methylated and unmethylated genes. Methylated genes were further divided into five groups based on the methylation level in their gene body (20% quintiles).

Figure 4. *Continued*
(C) Correlations between season-biased differentially expressed genes (DEGs) and differentially methylated regions (DMRs).
(D) Venn diagram of season-biased DMGs and DEGs in the liver.
(E) Expression levels of DEGs *CYP39A* (liver), *KLHL40* (skeletal muscle), *NCOR2* (liver), *GOT2* (adipose), *CATA2* (spleen), and *SHMT1* (liver) and methylation levels in the corresponding DMRs.

DMGs in most tissues ($q < 0.05$), except the kidneys ($q = 0.054$) (Figure 4C), suggesting that DNA methylation does regulate transcription. Some genes involved in physiological function regulation in hibernation exhibited altered methylation. For example, *CYP39A* transcription was significantly suppressed in the liver during hibernation, with a hyper differentially methylated region (DMR) from promoter to gene body (Figure 4D). Both *HLHL40* and *NCOR2* were hypermethylated in the gene body, but *HLHL40* was downregulated in hibernating skeletal muscle, whereas *NCOR2* was upregulated in the liver (Figure 4D). These results indicated that DNA methylation is, at least in part, responsible for adaptive transcriptional changes during hibernation, but its roles are much more complicated than previously realized. Indeed, the correlations between hyper- and hypo-DMGs, and down- and upregulated DEGs, were substantially more complex than anticipated. For example, 45 genes were hypermethylated and downregulated, whereas 31 genes were hypomethylated and upregulated in the liver during hibernation. However, 31 hyper-DMGs and 46 hypo-DMGs were up- and downregulated, respectively (Figure 4E).

Furthermore, a large number of DEGs (2,197) did not overlap with DMGs (Figure 4E), suggesting that seasonal changes in the expression of these genes may not be directly regulated by DNA methylation but rather result from methylation-dependent alterations in transcription networks.

DNA Methylation Alterations in TFs and Their Regulatory Networks during Hibernation

To investigate the role of methylation alterations in gene regulatory networks during hibernation, we subjected the season-biased DMGs to GO analysis, which revealed that, in nearly all tissues, GO terms referring to regulation of gene expression and metabolic process were significantly enriched ($q < 0.05$) in season-biased DMGs (Figure 5A). We identified 1,370 transcription factor (TF) genes in the Chinese alligator genome and analyzed them in relation to seasonal DMGs in each tissue. The observed ratio of differentially methylated TFs versus DMGs was significantly higher than expected (1,370/27,500) (Fisher's exact test, $q < 0.05$) (Figure 5B), suggesting that genes involved in gene expression regulation, especially TF genes, are more likely to be differentially methylated. To explore methylation-dependent regulatory networks in the hibernating Chinese alligator, we identified differentially expressed TFs with DMRs in each tissue (Figure 5C). Furthermore, we performed weighted gene co-expression network analysis (WGCNA) based on transcriptome data and constructed methylation-dependent regulatory networks for each tissue (Figures 5D, 5E, and S5). Most of the season-biased DEGs were regulated by the differentially methylated TFs in the transcription networks.

miRNA Regulation during Hibernation

miRNAs reportedly play a crucial role in gene expression regulation during hibernation (Arfat et al., 2018; Biggar and Storey, 2015; Lyons et al., 2013). Thus, we carried out sRNA-seq using adipose, brain, heart, small intestine, muscle, and gonad tissues to identify season-biased differentially expressed miRNAs (DEmiRs, $q < 0.05$). Some hibernation-related miRNAs are conserved and play roles in other hibernators. For example, miR-103, miR-124 (brain), and miR-206 (skeletal muscle) were upregulated in the hibernating alligator (Figure 6A), and these expression changes were also reported in corresponding tissues of the hibernating little brown bat (*Myotis lucifugus*) (Biggar and Storey, 2014a; Kornfeld et al., 2012). We also discovered new hibernation-related miRNAs, some of which are specific to the Chinese alligator (Figure 6A). The roles of miRNAs in gene expression regulation were found to be tissue specific. Their expression levels varied in different tissues during hibernation (Figures 6B–6D). For example, miR-10b was upregulated in the small intestine and adipose tissues during hibernation but downregulated in the brain, heart, muscle, and ovaries (Figure 6C). Similar patterns were observed for miR-1a and miR-19a (Figures 6B and 6D). Furthermore, the expression patterns suggested that the roles of some miRNAs are species specific. MiR-200a was downregulated in the adipose tissues of the hibernating Chinese alligator (Figure 6A) but reportedly is upregulated in hibernating thirteen-lined ground squirrels (*Ictidomys tridecemlineatus*) (Wu et al., 2014). MiR-1a is upregulated in the muscle in several hibernators (Arfat et al., 2018; Biggar and Storey, 2015) but not in the Chinese alligator.

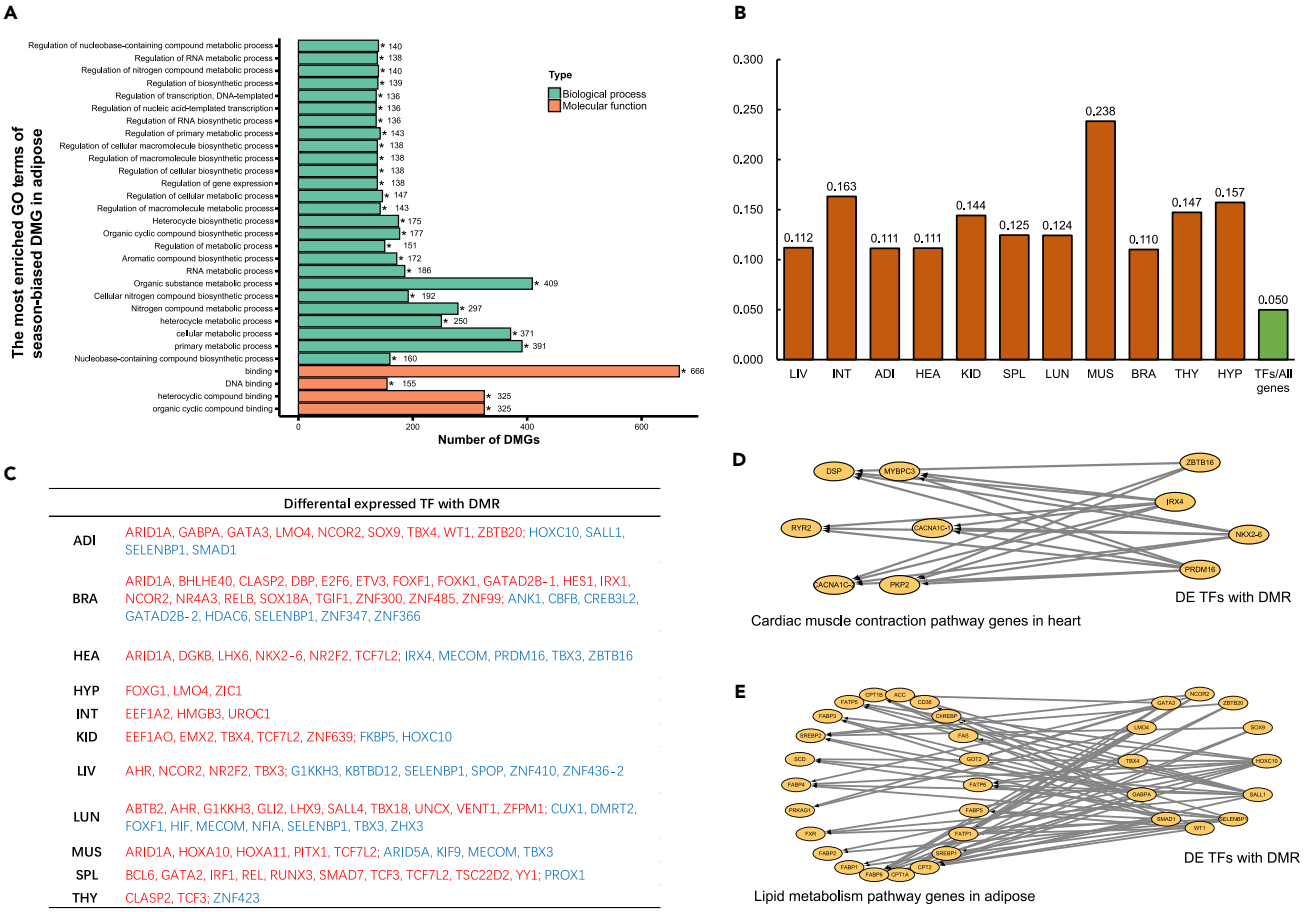

Figure 5. Regulation of Differentially Expressed and Differentially Methylated Transcription Factor (TF) Genes

(A) Thirty most enriched GO terms in season-biased differentially methylated genes (DMGs) in adipose tissues.

(B) Ratio of differentially methylated TF genes to DMGs.

(C) Correlation between differentially expressed TFs and DMRs.

(D and E) Associations between differentially expressed and differentially methylated TFs and cardiac muscle contraction pathway DEGs in the heart (D) and lipid metabolic pathway DEGs in adipose tissues (E).

See also Figure S5.

To explore the regulatory roles of annotated miRNAs during hibernation in the Chinese alligator, we predicted target genes of season-biased DEmiRs. Various genes involved in functional regulation during hibernation in each tissue were targeted by miRNAs (Table S5), including *DGAT1*, *DGAT2*, *APOA1*, *APOA4*, *APOB*, *ABCG8*, *CD36*, *MTTP1*, *MTTP2*, *FABP2* and *SCARB1*, which are related to fat digestion and absorption and were downregulated in the small intestine (Figure 6E), and *LPL*, *FATP6*, *SCD*, and *GOT2*, which are related to lipid metabolism and were downregulated in adipose tissues during hibernation (Figure 6F). One gene could be regulated by multiple miRNAs and, conversely, one miRNA could target multiple genes, thus forming a complex regulatory network (Figures 6E and 6F).

DISCUSSION

Although hibernation in ectotherms seems quite similar to that in endotherms, they are quite different in behavioral, physiological, and biochemical traits (Grigg and Kirshner, 2015; Staples, 2016). In hibernating mammals, the metabolic rate is suppressed during winter, along with a decrease in the core body temperature, which results in substantial energy saving (Hampton et al., 2013; Staples, 2016); however, periodic interbout arousals during hibernation still consume much energy (Karpovich et al., 2009). On the other hand, ectotherm hibernators exhibit continuous metabolic suppression exceeding the passive thermal effects due to a decrease in the environmental temperature in winter (Grigg and Kirshner, 2015; Staples, 2016).

A

	Season-biased	Season-biased expressed miRNA
ADI	Winter-biased	let-7c, miR-10b, 99a, 100, 122, 148a, 196a-1, 196a-2, 196a-3, 202, 206, 215-2, 458,
	Summer-biased	miR-1a, 9a, 15a, 15c, 16a, 16b, 17, 19a, 19b, 20a, 20b, 93a, 29b, 29c, 30a, 30e, 32, 34a, 106a, 128, 130, 133a, 135, 142a, 146a, 146b, 155, 190a, 200a, 215-1, 218, 363, 383, 429, 454, 460a, 499b, 1388a, 2188, miR-novel123, novel1267, novel108
BRA	Winter-biased	lin-4, miR-7a, 7b, 9a, 9b, 15a, 15b, 15c, 16a, 16b, 17, 18b, 19a, 19b, 29b, 29c, 20a, 20b, 30b, 30e, 31, 32, 34b, 34c, 93a, 98, 103a, 103b, 106a, 122, 124a, 124b, 125a, 128, 130, 137, 138a, 138b, 1397, 142a, 144, 150, 153,1662, 1805,191, 193b, 194-2, 200a, 200b, 202, 204, 216a, 2184a, 2184b, 219a, 221, 222a, 222b,301a, 301b, 365, 375, 383, 429, 449a, 454, 458, 459, 460a, 489, miR-novel1086, novel1278, novel129, novel1399, novel210, novel220, novel234, novel274, novel371
	Summer-biased	let-7e, miR-1a, 1b, 10a, 10b, 10c, 34a, 126a, 126b, 143, 146a, 146c, 148a, 1791, 182, 183, 206, 218, 219b, 338, 455, miR-novel123, novel182, novel235, novel283, novel790, novel886, novel900, novel985
HEA	Winter-biased	lin-4, 133b, 144, 146b, 152, 199a, 223, 2188
	Summer-biased	miR-10a, 10b, 139, 187, miR-novel113
INT	Winter-biased	let-7a, 7c, 7e, 7f, 1a, 1b, 10b, 23b, 30d, 99a, 100, 101, 143, 145, 148a, 187, 2184a, novel123, novel169, novel185, novel770
	Summer-biased	miR-9a, 15a, 15b-1, 15b-2, 15c, 16a, 16b, 17, 19a, 19b, 20a, 20b, 29c, 30a, 30c, 30e, 31, 32, 33-1,92a, 93a, 98, 103b, 106a, 128, 142a, 146b, 147, 150, 155, 181a, 181b, 191, 192a, 194-1, 194-2, 199a, 200a, 200b, 210, 214, 215-1, 215-2, 221, 222a, 222b, 223, 363, 375, 429, 454, 456, 458, 459, 460a, 1662, 9609, miR-novel113, novel1377, novel1450, novel167
MUS	Winter-biased	miR-7a, 199a, 206, 2184a
	Summer-biased	miR-10b, 100, 187, 499b

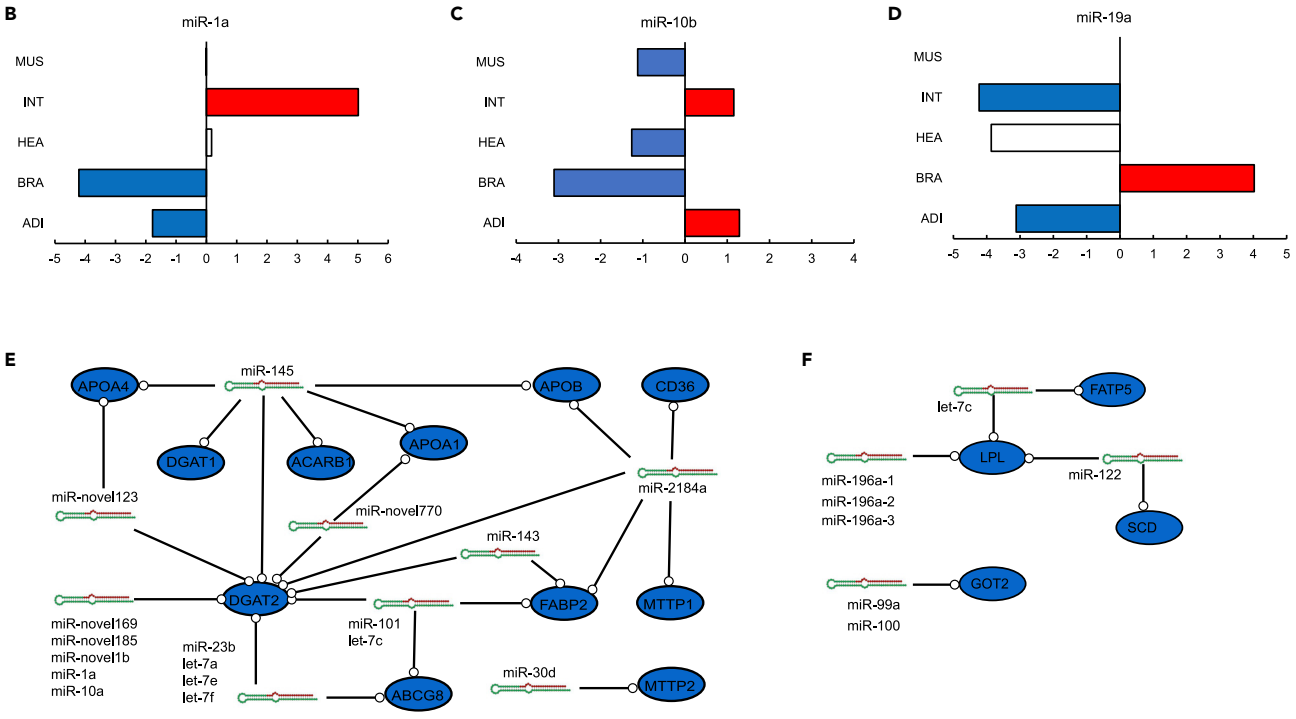

Figure 6. MiRNA Regulation of Gene Expression during Chinese Alligator Hibernation

(A) Functional key genes targeted by season-biased differentially expressed miRNAs (DEmiRs) in each tissue.

(B–D) Seasonal expression changes for miR-1a (B), miR-10b (C), and miR-19a (D).

(E and F) Relations between DEmiRs and differentially expressed genes (DEGs) in fat digestion and absorption in the small intestine (E) and lipid metabolic pathway genes in adipose tissues (F).

See also Table S5.

In mammals, the entering of hibernation is accompanied by a switch of fuel use from carbohydrates to lipids, which provide the most energy-dense metabolic substrate (Sheriff et al., 2013). Previous transcriptome studies in hibernating mammals have provided molecular evidences for this switch. For example, in the white adipose tissue of hibernating free-ranging dwarf lemurs in a wild population, several genes involved in lipid catabolism (e.g., *PLPP1*, *APOC2*, *SCD*, *FASN*, and *ELOVL6*) and carbohydrate oxidation repression (*PDK4*) were induced, whereas several genes involved in carbohydrate catabolism (e.g., *PDHA1*, *PDHB*, *DLAT*, and *DLD*) were downregulated (Faherty et al., 2018). In the brown adipose tissue of hibernating thirteen-lined ground squirrel, many genes participating in lipolysis (e.g., *PNPLA2*, *PLIN2*, *PLIN4*, and *PLIN5*) and lipid transport (e.g., *OBP2B, FABP3*, *SLC25A20*, *CPT1A*, and *CPT2*), as well as *PDK4* are upregulated (Hampton et al., 2013). In addition, in the past three decades, many studies on gene expression, epigenetic regulation, proteins, enzymes, and posttranslational modification have provided evidence supporting the switch of fuel use in mammalian hibernators (Carey et al., 2003; Staples, 2016).

The main energy source and the energy-saving strategy of hibernating ectotherms are still unclear. Similar to mammal hibernators, the common lizard (*Lacerta vivipara*) and gecko (*Phyllodactylus marmoratus*) reportedly rely on fat stores during hibernation (Avery, 1970; Daniels, 1984), whereas another study suggested that glycogen, not lipids, limits winter survival of side-blotched lizards (*Uta stansburiana*) (Zani et al., 2012). Both liver- and muscle-stored glycogens are substantially consumed during hibernation and considerably account for the winter energy budget of several lizard and snake species (Costanzo, 1985; Dessauer, 1953; Zani et al., 2012). Transcriptomic studies on the heart, skeletal muscle, and kidneys/brain of Chinese alligator and Australian central bearded dragon have identified candidate genes and pathways that are involved in seasonal adaption and tissue-specific function maintenance and have provided valuable insights into the molecular regulatory mechanism underlaying reptile hibernation (Capraro et al., 2019; Sun et al., 2018). In our study, we extend the analysis to other important tissues, including the brain, hypothalamus (central control), thyroid gland (metabolism regulation), small intestine (nutrient digestion and absorption), liver (metabolism), adipose (energy storage), lung (gas exchange), heart (blood supply), skeletal muscle (movement), and spleen (immunity), to provide a comprehensive transcriptome profile of the hibernating reptile.

Our data revealed a unique energy-saving strategy in the hibernating Chinese alligator during hibernation. Adapting to the fasting state, the hibernating alligator suppressed pathways related to nutrition absorption and metabolism. Overall, genes in fat catabolism pathways were dramatically downregulated in the hibernating Chinese alligator, except for liver *CPT1A*, which was significantly upregulated, suggesting that the fat metabolism pathways are generally suppressed instead of activated during alligator hibernation. However, β-oxidation of FA in the liver, but not in the muscle, was activated to use the limited FAs, ensuring the energy demands of the liver as the metabolic center. This is supported by our finding during tissue collection that the amount of adipose tissue did not differ significantly between winter and summer. In addition, glycogen phosphorylase genes were not downregulated like other genes in carbohydrate metabolism; instead, the muscle glycogen phosphorylase gene *GYPM* was considerably upregulated ($q = 6.85 \times 10^{-36}$, fold change = 1.48), suggesting that glycogen, especially that stored in muscle, may be another reserve energy source of the hibernating Chinese alligator. Our results provide molecular evidence that glycogenolysis in muscle and β-oxidation of hepatic FA supply scarce energy for the hibernating Chinese alligator with suppressed carbohydrate and fat catabolism. Through downregulation of thyrotropin-releasing hormone gene and its downstream thyroid hormone biosynthesis pathway, nutrition absorption and metabolism, cardiac and show skeletal muscle contraction, and urinary excretion and immunity function pathways were also generally downregulated during hibernation, reflecting a coordinated suppression of the metabolic rate and physiological states. However, a few upregulated genes in these pathways, for example, *CPT1A* and *AMPK*, which, respectively, catalyze FA catabolism and inhibit FA synthesis in the liver, as well as upregulated genes involved in fast muscle fiber contraction (*TNNC2, MYL1,* and *MYH3*), reveal the ingenious energy utilization and survival strategies in this species.

In Australian central bearded dragon, the enrichment of "lipid catabolic processes" and "carbohydrate catabolic processes" GO terms in downregulated genes suggest an overall suppression of lipid and carbohydrate catabolism, but the upregulation of carbohydrate metabolism genes, such as *PFKFB3*, *GSK3A*, and *FBP1*, which are important in glycolysis, glycogen synthesis, and gluconeogenesis, respectively, indicates a different strategy of fuel use and energy saving (Capraro et al., 2019). Using seasonal transcriptome data from the kidneys, skeletal muscle, and heart in the Chinese alligator reported by another research group (Sun et al., 2018), we were able to explore whether the adaptive mechanisms are similar between the only two Chinese alligator populations. We identified five DEGs (62.5%) among the eight seasonal DEGs reported in their study, including *CSRP3*, *AT1A1*,

PCKGC, *KCRB*, and *CIRBP*. In addition, the two datasets share many of the KEGG pathways enriched in seasonal DEGs. These results support the repeatability and universality of our data.

DNA methylation reportedly plays an important role in the regulation of gene expression associated with mammalian hibernation (Alvarado et al., 2015; Biggar and Storey, 2014b; Fujii et al., 2006). TFs read DNA methylation and translate the information into certain gene expression patterns (Buck-Koehntop and Defossez, 2013; Zhu et al., 2016). TF genes themselves are also DNA methylation targets in various biological processes (Ivascu et al., 2007; Zinger et al., 2019). In thirteen-lined ground squirrels, the global DNA methylation level was increased in brown adipose tissue (Biggar and Storey, 2014b) but decreased in skeletal muscle (Alvarado et al., 2015). The CpG methylation level of the *MEF2C* promoter region correlated with the downregulation of gene expression in skeletal muscle of thirteen-lined ground squirrels (Alvarado et al., 2015). In chipmunk, CpG methylation in the USF-binding site is crucial for liver-specific transcription of the hibernation-specific gene, *HP-27* (Fujii et al., 2006). Although these studies provided a glance into the DNA regulation in hibernation, they largely focused on changes in overall DNA methylation levels or the methylation of specific genes. In this study, we carried out BS-seq, the gold standard for DNA methylation profiling with high resolution, in active and hibernating states. By combining transcriptome and methylome data, we found that *cis*- and *trans*-regulation of DNA methylation participates in gene transcription changes during hibernation. Although DMGs are likely to be differentially expressed, most DEGs are not directly regulated by DNA methylation changes but by differentially expressed TFs with DMRs. In this economical and ingenious strategy, reversible drastic transcriptome changes in the Chinese alligator are regulated by modulating the transcription of TF genes. These results are consistent with observations in other hibernators, where numerous TFs play important roles during hibernation, such as *HNF-1* in the chipmunk (*Tamias asiaticus*) (Ono et al., 2001), *ATF4* and *NFAT* in the thirteen-lined ground squirrel (Mamady and Storey, 2008; Zhang and Storey, 2016), *ZBED1* in the greater horseshoe bat (*Rhinolophus ferrumequinum*) (Xiao et al., 2016), and *HSF* in the red-eared slider turtle (*Trachemys scripta elegans*) (Krivoruchko and Storey, 2010).

Overall, our results provide insights into the genetic and epigenetic mechanisms underlying hibernation in the Chinese alligator and are expected to facilitate the development of scientific programs for successful conservation of this endangered species.

Limitations of the Study

This study revealed the suppression of metabolic rate and physiological states of hibernating Chinese alligator and suggested a unique energy-saving strategy that differs from that in hibernating mammals. Although we found that the downregulation of thyroid hormone biosynthesis plays an important regulatory role during this process, more investigations are needed to identify the core "hibernation factor," which triggers and turns off the hibernation state. In addition, similar omics study should be done on more hibernating ectotherms to further explore the evolution of hibernation regulation in hibernating animals including reptiles as well as other ectotherms.

Resource Availability

Lead Contact

Further information and requests for resources should be directed to and will be fulfilled by the Lead Contact, Sheng-Guo Fang (sgfanglab@zju.edu.cn).

Materials Availability

The study did not generate new unique reagents.

Data and Code Availability

The Chinese alligator reference genome is available in the NCBI with the assembly accession number GCA_000455745.1. The BS-seq, mRNA-seq, and sRNA-seq data generated in this work have been deposited in the SRA database under NCBI BioProjects: PRJNA556094, PRJNA556093, and PRJNA556092, respectively. The iTRAQ and TMT data have been deposited in the ProteomeXchange with identifier PXD019278 and PXD019277, respectively. The DNA methylome data of *Petromyzon marinus*, *Danio rerio*, *Bos grunniens*, *Homo sapiens*, and *Gallus gallus* were downloaded from NCBI SRA database: SRR2457525, SRR800080, SRR8834688, SRR3427332, and SRR5003428, respectively.

METHODS

All methods can be found in the accompanying Transparent Methods supplemental file.

SUPPLEMENTAL INFORMATION

Supplemental Information can be found online at https://doi.org/10.1016/j.isci.2020.101202.

ACKNOWLEDGMENTS

We would like to thank Prof. M. Thomas P. Gilbert (the University of Copenhagen) for his help modifying the manuscript. We would also like to thank Xuan-Min Guang (Zhejiang University) for his help with data analysis. We would like to thank Li-Ming Fang, Zhen-Wei Wang, Wei-Qiang Zou, Da-Bin Ren, and Ju-Min Xu (Changxing Yinjiabian Chinese Alligator Nature Reserve) for their help in sample collection. This work was supported by the Key Program of the National Natural Science Foundation of China (31530087) and the National Key Program (2016YFC0503200) from the Ministry of Science and Technology of China.

AUTHOR CONTRIBUTIONS

Conceptualization, S.-G.F. and Q.-H.W.; Methodology, Q.-H.W. and J.-Q.L.; Investigation and Formal Analysis, J.-Q.L., Y.-Y.H., M.-Y.B., Q.-H.W., and S.-G.F.; Resources, S.-G.F.; Writing – Original Draft Preparation, J.-Q.L, M.-Y.B, Q.-H.W., and S.-G.F.; Writing – Review & Editing, J.-Q.L., Y.-Y.H., Q.-H.W., and S.-G.F.; Supervision, S.-G.F. and Q.-H.W.; Project Administration and Funding Acquisition, S.-G.F.

DECLARATION OF INTERESTS

The authors declare no competing interests.

Received: February 14, 2020
Revised: April 16, 2020
Accepted: May 22, 2020
Published: June 26, 2020

REFERENCES

Alvarado, S., Mak, T., Liu, S., Storey, K.B., and Szyf, M. (2015). Dynamic changes in global and gene-specific DNA methylation during hibernation in adult thirteen-lined ground squirrels, Ictidomys tridecemlineatus. J. Exp. Biol. *218*, 1787–1795.

Ambros, V. (2004). The functions of animal microRNAs. Nature *431*, 350–355.

Arfat, Y., Chang, H., and Gao, Y. (2018). Stress-responsive microRNAs are involved in re-programming of metabolic functions in hibernators. J. Cell Physiol. *233*, 2695–2704.

Avery, R.A. (1970). Utilization of caudal fat by hibernating common lizards, *LacertaVivipara*. Comp. Biochem. Physiol. *37*, 119–121.

Biggar, K.K., and Storey, K.B. (2014a). Identification and expression of microRNA in the brain of hibernating bats, *Myotis lucifugus*. Gene *544*, 67–74.

Biggar, K.K., and Storey, K.B. (2015). Insight into post-transcriptional gene regulation: stress-responsive microRNAs and their role in the environmental stress survival of tolerant animals. J. Exp. Biol. *218*, 1281–1289.

Biggar, Y., and Storey, K.B. (2014b). Global DNA modifications suppress transcription in brown adipose tissue during hibernation. Cryobiology *69*, 333–338.

Breiling, A., and Lyko, F. (2015). Epigenetic regulatory functions of DNA modifications: 5-methylcytosine and beyond. Epigenetics Chromatin. *8*, 24.

Britton, C.H., Mackey, D.W., Esser, V., Foster, D.W., Burns, D.K., Yarnall, D.P., Froguel, P., and McGarry, J.D. (1997). Fine chromosome mapping of the genes for human liver and muscle carnitine palmitoyltransferase I (CPT1A and CPT1B). Genomics *40*, 209–211.

Buck-Koehntop, B.A., and Defossez, P.A. (2013). On how mammalian transcription factors recognize methylated DNA. Epigenetics *8*, 131–137.

Capraro, A., O'Meally, D., Waters, S.A., Patel, H.R., Georges, A., and Waters, P.D. (2019). Waking the sleeping dragon: gene expression profiling reveals adaptive strategies of the hibernating reptile *Pogona vitticeps*. BMC Genomics *20*, 460.

Carey, H.V., Andrews, M.T., and Martin, S.L. (2003). Mammalian hibernation: cellular and molecular responses to depressed metabolism and low temperature. Physiol. Rev. *83*, 1153–1181.

Chen, B.H., Hua, T.M., Wu, X.B., and Wang, C.L. (2003). Research on Chinese Alligator (Shanghai Scientific and Technological Education Publishing House).

Cooper, S.T., Sell, S.S., Fahrenkrog, M., Wilkinson, K., Howard, D.R., Bergen, H., Cruz, E., Cash, S.E., Andrews, M.T., and Hampton, M. (2016). Effects of hibernation on bone marrow transcriptome in thirteen-lined ground squirrels. Physiol. Genomics *48*, 513–525.

Costanzo, J.P. (1985). The bioenergetics of hibernation in the eastern garter snake *Thamnophis sirtalis sirtalis*. Physiol. Zool. *58*, 682–692.

Daniels, C.B. (1984). The importance of caudal lipid in the gecko *Phyllodactylus marmoratus*. Herpetologica *40*, 337–344.

Dessauer, H.C. (1953). Hibernation of the lizard, *Anolis carolinensis*. Proc. Soc. Exp. Biol. Med. *82*, 351–353.

Faherty, S.L., Villanueva-Canas, J.L., Blanco, M.B., Alba, M.M., and Yoder, A.D. (2018). Transcriptomics in the wild: hibernation physiology in free-ranging dwarf lemurs. Mol. Ecol. *27*, 709–722.

Faherty, S.L., Villanueva-Canas, J.L., Klopfer, P.H., Alba, M.M., and Yoder, A.D. (2016). Gene expression profiling in the hibernating primate, *Cheirogaleus medius*. Genome Biol. Evol. *8*, 2413–2426.

Fang, L.M., Zhai, T., Zhao, L., and Fang, S.G. (2015). Deep brumation features of Zhejiang Chinese alligators. Chin. J. Wildl. *36*, 284–287.

Fujii, G., Nakamura, Y., Tsukamoto, D., Ito, M., Shiba, T., and Takamatsu, N. (2006). CpG methylation at the USF-binding site is important for the liver-specific transcription of the chipmunk *HP-27* gene. Biochem. J. *395*, 203–209.

Grigg, G.C., and Kirshner, D. (2015). Biology and Evolution of Crocodylians (Comstock Publishing Associates a division of Cornell University Press).

Hampton, M., Melvin, R.G., and Andrews, M.T. (2013). Transcriptomic analysis of brown adipose tissue across the physiological extremes of natural hibernation. PLoS One *8*, e85157.

Herbert, C.V., and Jackson, D.C. (1985). Temperature effects on the responses to prolonged submergence in the turtle *Chrysemys Picta Bellii* .2. Metabolic-rate, blood acid-base and ionic changes, and cardiovascular function in aerated and anoxic water. Physiol. Zool. *58*, 670–681.

Humphries, M.M., Thomas, D.W., and Speakman, J.R. (2002). Climate-mediated energetic constraints on the distribution of hibernating mammals. Nature *418*, 313–316.

Inouye, D.W., Barr, B., Armitage, K.B., and Inouye, B.D. (2000). Climate change is affecting altitudinal migrants and hibernating species. Proc. Natl. Acad. Sci. U S A *97*, 1630–1633.

Ivascu, C., Wasserkort, R., Lesche, R., Dong, J., Stein, H., Thiel, A., and Eckhardt, F. (2007). DNA methylation profiling of transcription factor genes in normal lymphocyte development and lymphomas. Int. J. Biochem. Cell Biol. *39*, 1523–1538.

Jones, P.A. (2012). Functions of DNA methylation: islands, start sites, gene bodies and beyond. Nat. Rev. Genet. *13*, 484–492.

Karpovich, S.A., Toien, O., Buck, C.L., and Barnes, B.M. (2009). Energetics of arousal episodes in hibernating arctic ground squirrels. J. Comp. Physiol. B *179*, 691–700.

Kornfeld, S.F., Biggar, K.K., and Storey, K.B. (2012). Differential expression of mature microRNAs involved in muscle maintenance of hibernating little brown bats, *Myotis lucifugus*: a model of muscle atrophy resistance. Genomics Proteomics Bioinformatics *10*, 295–301.

Krivoruchko, A., and Storey, K.B. (2010). Regulation of the heat shock response under anoxia in the turtle, *Trachemys scripta elegans*. J. Comp. Physiol. B *180*, 403–414.

Lei, M., Dong, D., Mu, S., Pan, Y.H., and Zhang, S. (2014). Comparison of brain transcriptome of the greater horseshoe bats (*Rhinolophus ferrumequinum*) in active and torpid episodes. PLoS One *9*, e107746.

Luan, Y., Ou, J., Kunze, V.P., Qiao, F., Wang, Y., Wei, L., Li, W., and Xie, Z. (2018). Integrated transcriptomic and metabolomic analysis reveals adaptive changes of hibernating retinas. J. Cell Physiol. *233*, 1434–1445.

Lyons, P.J., Lang-Ouellette, D., and Morin, P., Jr. (2013). CryomiRs: towards the identification of a cold-associated family of microRNAs. Comp. Biochem. Physiol. Part D Genomics Proteomics *8*, 358–364.

Mamady, H., and Storey, K.B. (2008). Coping with the stress: expression of ATF4, ATF6, and downstream targets in organs of hibernating ground squirrels. Arch. Biochem. Biophys. *477*, 77–85.

Mateju, K., Bendova, Z., El-Hennamy, R., Sladek, M., Sosniyenko, S., and Sumova, A. (2009). Development of the light sensitivity of the clock genes *Period1* and *Period2*, and immediate-early gene *c-fos* within the rat suprachiasmatic nucleus. Eur. J. Neurosci. *29*, 490–501.

Nespolo, R.F., Gaitan-Espitia, J.D., Quintero-Galvis, J.F., Fernandez, F.V., Silva, A.X., Molina, C., Storey, K.B., and Bozinovic, F. (2018). A functional transcriptomic analysis in the relict marsupial *Dromiciops gliroides* reveals adaptive regulation of protective functions during hibernation. Mol. Ecol. *27*, 4489–4500.

Oaks, J.R. (2011). A time-calibrated species tree of Crocodylia reveals a recent radiation of the true crocodiles. Evolution *65*, 3285–3297.

Ono, M., Hosoe, Y., Azuma, S., Shoji, M., Nara, K., Kondo, N., Shiba, T., and Takamatsu, N. (2001). HNF-1 regulates the liver-specific transcription of the chipmunk *HP-20* gene. Gene *277*, 121–127.

Pelizzola, M., and Ecker, J.R. (2011). The DNA methylome. FEBS Lett. *585*, 1994–2000.

Saito, T., Sugimoto, K., Adachi, Y., Wu, Q., and Mori, K.J. (2000). Cloning and characterization of amphibian cold inducible RNA-binding protein. Comp. Biochem. Physiol. B Biochem. Mol. Biol. *125*, 237–245.

Sheriff, M.J., Fridinger, R.W., Toien, O., Barnes, B.M., and Buck, C.L. (2013). Metabolic rate and prehibernation fattening in free-living arctic ground squirrels. Physiol. Biochem. Zool. *86*, 515–527.

Smith, Z.D., and Meissner, A. (2013). DNA methylation: roles in mammalian development. Nat. Rev. Genet. *14*, 204–220.

Staples, J.F. (2016). Metabolic flexibility: hibernation, torpor, and estivation. Compr. Physiol. *6*, 737–771.

Storey, K.B. (1996). Metabolic adaptations supporting anoxia tolerance in reptiles: recent advances. Comp. Biochem. Physiol. B Biochem. Mol. Biol. *113*, 23–35.

Storey, K.B. (2006). Reptile freeze tolerance: metabolism and gene expression. Cryobiology *52*, 1–16.

Storey, K.B., and Storey, J.M. (2007). Tribute to P. L. Lutz: putting life on 'pause' – molecular regulation of hypometabolism. J. Exp. Biol. *210*, 1700–1714.

Storey, K.B., and Storey, J.M. (2013). Molecular biology of freezing tolerance. Compr. Physiol. *3*, 1283–1308.

Su, Z., Han, L., and Zhao, Z. (2011). Conservation and divergence of DNA methylation in eukaryotes: new insights from single base-resolution DNA methylomes. Epigenetics *6*, 134–140.

Sugimoto, K., and Jiang, H.J. (2008). Cold stress and light signals induce the expression of cold-inducible RNA binding protein (cirp) in the brain and eye of the Japanese treefrog (*Hyla japonica*). Comp. Biochem. Physiol. A Mol. Integr. Physiol. *151*, 628–636.

Sun, H.J., Zuo, X.B., Sun, L., Yan, P., Zhang, F., Xue, H., Li, E., Zhou, Y.K., Wu, R., and Wu, X.B. (2018). Insights into the seasonal adaptive mechanisms of Chinese alligators (*Alligator sinensis*) from transcriptomic analyses. Aust. J. Zool. *66*, 93–102.

Wan, Q.H., Pan, S.K., Hu, L., Zhu, Y., Xu, P.W., Xia, J.Q., Chen, H., He, G.Y., He, J., and Ni, X.W. (2013). Genome analysis and signature discovery for diving and sensory properties of the endangered Chinese alligator. Cell Res. *23*, 1091–1105.

Wu, C.W., Biggar, K.K., and Storey, K.B. (2014). Expression profiling and structural characterization of microRNAs in adipose tissues of hibernating ground squirrels. Genomics Proteomics Bioinformatics *12*, 284–291.

Xia, T.S., Zhu, J.L., and Shao, M. (2006). Relationship between temperature and diseases occurrence of Chinese alligator during hibernation. Sichuan J. Zool *25*, 400–402.

Xiao, Y., Wu, Y., Sun, K., Wang, H., Jiang, T., Lin, A., Huang, X., Yue, X., Shi, L., and Feng, J. (2016). Gene expression and adaptive evolution of *ZBED1* in the hibernating greater horseshoe bat (*Rhinolophus ferrumequinum*). J. Exp. Biol. *219*, 834–843.

Zani, P.A., Irwin, J.T., Rollyson, M.E., Counihan, J.L., Healas, S.D., Lloyd, E.K., Kojanis, L.C., Fried, B., and Sherma, J. (2012). Glycogen, not dehydration or lipids, limits winter survival of side-blotched lizards (*Uta stansburiana*). J. Exp. Biol. *215*, 3126–3134.

Zhang, G.L., Geng, Y.J., Xlao, J.G., and Yang, S.H. (2003). Comparison of two overwintering ways for Chinese alligator in captivity. J. Econ. Anim. *7*, 57–59.

Zhang, Y., and Storey, K.B. (2016). Regulation of gene expression by NFAT transcription factors in hibernating ground squirrels is dependent on the cellular environment. Cell Stress Chaperones *21*, 883–894.

Zhu, H., Wang, G.H., and Qian, J. (2016). Transcription factors as readers and effectors of DNA methylation. Nat. Rev. Genet. *17*, 551–565.

Zinger,L.,Bonin,A.,Alsos,I.G.,Balint,M.,Bik,H.,Boyer, F.,Chariton,A.A.,Creer,S.,Coissac,E.,Deagle,B.E.,etal. (2019).DNAmetabarcoding-Needforrobust experimentaldesignstodrawsoundecological conclusions.Mol.Ecol.*28*,1857–1862.

iScience, Volume *23*

Supplemental Information

A Unique Energy-Saving Strategy during Hibernation Revealed by Multi-Omics Analysis in the Chinese Alligator

Jian-Qing Lin, Yun-Yi Huang, Meng-Yao Bian, Qiu-Hong Wan, and Sheng-Guo Fang

SUPPLEMENTARY FIGURES

A. Female

KEGG pathway	Gene number	Down-regulated DEGs Number	Down-regulated DEGs q value	Up-regulated DEGs Number	Up-regulated DEGs q value	Key genes
Liver						
Primary bile acid biosynthesis	14	7	0.011	0	/	*CYP39A1, HSD3B7, AKR1D1, HSD17B4, BAAT*
Bile secretion	79	14	0.139	2	1.000	*SCARB1, NCEH1, EPHX1, BAAT, AQP9, ABCB1, FXR*
Small intestine						
Fat digestion and absorption	26	16	4.024E-05	1	1.000	*CD36, SCARB1, NPC1L1, FABP1, FABP2, MGAT2, DGAT1, DGAT2, MTTP, APOB, APOA4, APOA1*
Vitamin digestion and absorption	16	8	0.018	0	/	*THTR, RFC1, SCARB1, APOB, APOA4, APOA1, IF, CUBN*
Carbohydrate digestion and absorption	35	8	0.211	2	1.000	*LCT, MGAM, SGLT1,G6PC,GLUT5*
Mineral absorption	32	10	0.046	0	/	*DAR,SLC26A9, ZIP4, CTR1, SGLT1, FPN1, ATP1A, ATP1B, HEPH, NRAMP*
Protein digestion and absorption	87	15	0.210	1	1.000	*PEPT1, XPNPEP2, LAT2, TAT1, ATP1A, ATP1B*

B. Male

KEGG pathway	Gene number	Down-regulated DEGs Number	Down-regulated DEGs Enrichment	Up-regulated DEGs Number	Up-regulated DEGs Enrichment	Key genes
Liver						
Primary bile acid biosynthesis	14	5	0.183	1	1.000	*CYP39A1, CYP27A, AKR1D1, HSD17B4, BAAT*
Bile secretion	79	13	0.337	6	1.000	*SCARB1, NCEH1, EPHX1, BAAT, AQP1, ABCB1*
Small intestine						
Fat digestion and absorption	26	17	1.172E-04	1	1.000	*CD36, SCARB1, NPC1L1, FABP1, FABP2, MGAT2, DGAT1, DGAT2, MTTP, APOB, APOA4, APOA1*
Vitamin digestion and absorption	16	7	0.117	0	/	*RBP2, SCARB1, APOB, APOA4, APOA1, IF, CUBN*
Carbohydrate digestion and absorption	35	9	0.286	2	1.000	*LCT, MGAM, SGLT1,G6PC,GLUT5*
Mineral absorption	32	12	0.085	0	/	*DAR,SLC26A9, VDR, CTR1, SGLT1, FPN1, ATP1A, ATP1B, HEPH, NRAMP, FTH1*
Protein digestion and absorption	87	20	0.117	2	1.000	*MME, PEPT1, RBAT, LAT2, TAT1, ATP1A, ATP1B*

C. Heatmap

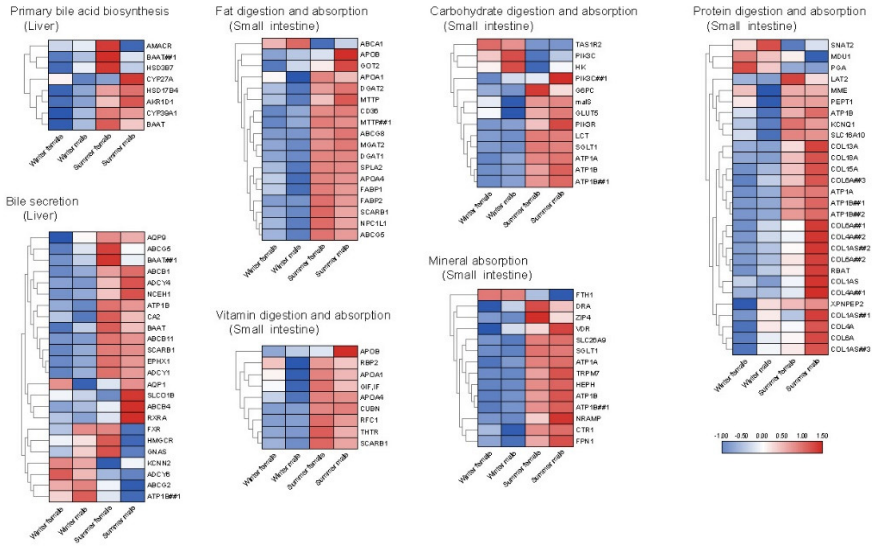

Figure S1. Gene expression patterns in key pathways involved in digestion and absorption in the liver and small intestine, Related to Figure 2. A, B. Season-biased differentially expressed genes (DEGs) in key pathways involved in nutrient digestion and absorption in the liver and small intestine in female (A) and male (B) Chinese alligators. **C.** Expression heatmap of seasonally DEGs in key pathways involved in digestion and absorption in the liver and small intestine.

A.

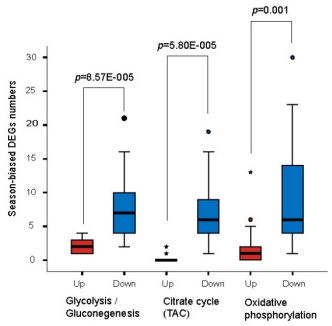

D.

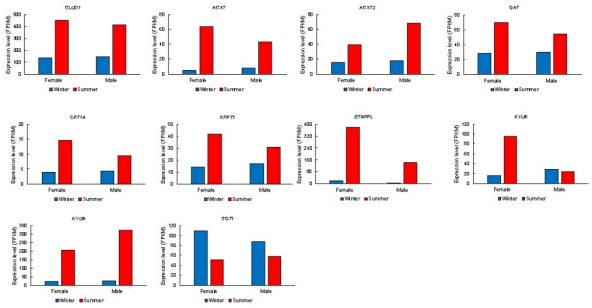

B.

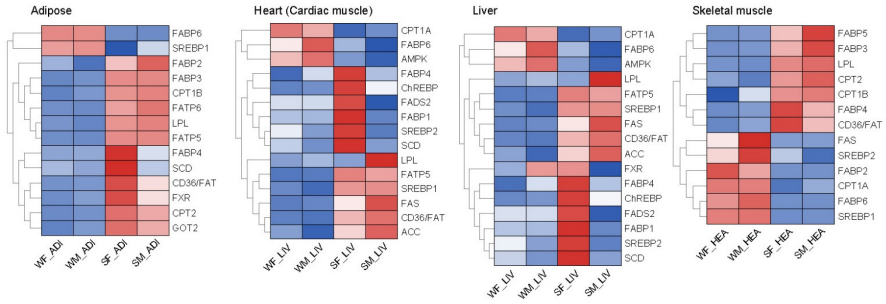

C.

	Female					Male				All			
	Total genes	All DEGs	Down DEGs	Up DEGs	q	All DEGs	Down DEGs	Up DEGs	q	All DEGs	Down DEGs	UP DEGs	q
Alanine, aspartate and glutamate metabolism	44	11	8	3		8	7	1		6	5	1	
Glycine, serine and threonine metabolism	33	14	14	0		11	11	0		6	6	0	
Cysteine and methionine metabolism	39	13	9	4		12	9	3		5	5	0	
Valine, leucine and isoleucine degradation	70	10	9	1	Wilcoxon signedrank test, Z=-2.814, q=0.005	13	11	2	Wilcoxon signedrank test, Z=-2.943, q=0.003	7	7	0	Wilcoxon signedrank test, Z=-2.608, q=0.009
Lysine degradation	46	10	8	2		6	6	0		3	3	0	
Arginine biosynthesis	16	6	3	3		3	2	1		1	0	1	
Arginine and proline metabolism	41	8	5	3		7	5	2		3	2	1	
Histidine metabolism	20	4	3	1		5	4	1		2	1	1	
Tyrosine metabolism	37	11	8	3		9	7	2		8	8	0	
Tryptophan metabolism	36	10	8	2		9	7	2		6	6	0	
Phenylalanine metabolism	18	5	3	2		2	2	0		1	1	0	

Figure S2. Gene expression patterns in key pathways involved in nutrient metabolism, Related to Figure 2. A. Box plots of season-biased differentially expressed gene (DEG) numbers in pathways involved in carbohydrate metabolism. **B.** Expression heatmap of season-biased DEGs involved in lipid metabolism in the liver, adipose tissues, cardiac muscle, and skeletal muscle. **C.** Numbers of DEGs in amino acid metabolic pathways in the liver. **D.** Expression patterns of genes crucial for amino acid metabolism.

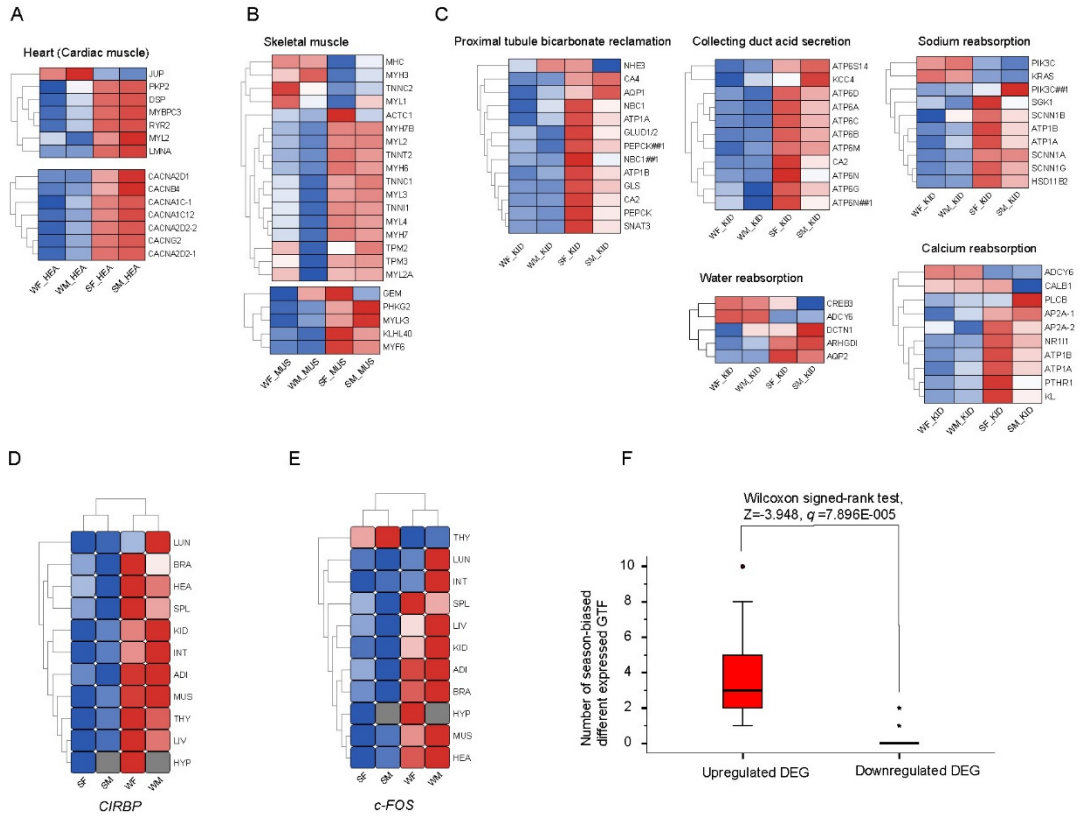

Figure S3. Gene expression patterns in key pathways involved in physiological function, Related to Figure 2. A, B, C. Heatmaps of differentially expressed genes (DEGs) involved in cardiac contraction and heart disease (A), skeletal muscle contraction and development (B), reabsorption and excretion in the kidneys (C). **D, E.** Expression patterns of *CIRBP* (D) and *c-FOS* (E). **F.** Comparison of the numbers of upregulated and downregulated general transcription factor genes (*GTF*s) during hibernation.

	mCG density			Methylation level of mCG			Methylation level of all CG		
	Summer	Winter	Wilcoxon signed-rank test	Summer	Winter	Wilcoxon signed-rank test	Summer	Winter	Wilcoxon signed-rank test
Adipose	97.19	95.35		77.84	74.86		79.32	77.42	
Brain	98.12	96.71		76.88	79.16		78.84	78.67	
Heart	97.58	95.21		74.74	71.55		77.15	75.16	
Hypothalamus	97.95	98.84		66.05	49.27		80.08	78.23	
Small intestine	97.50	96.28		74.70	72.59		75.89	73.58	
Kidney	98.43	98.29	Z=-1.778 q=0.083	80.15	77.73	Z=-1.423 q=0.155	81.97	79.45	Z=-1.867 q=0.067
Skeletal muscle	97.51	97.14		77.96	78.30		74.92	74.67	
Liver	98.05	97.00		74.98	78.56		77.58	78.67	
Lung	98.31	98.26		79.07	78.82		80.17	81.19	
Spleen	98.45	98.51		81.62	79.20		82.91	80.63	
Thyroid	97.72	98.74		80.68	79.43		80.87	81.32	

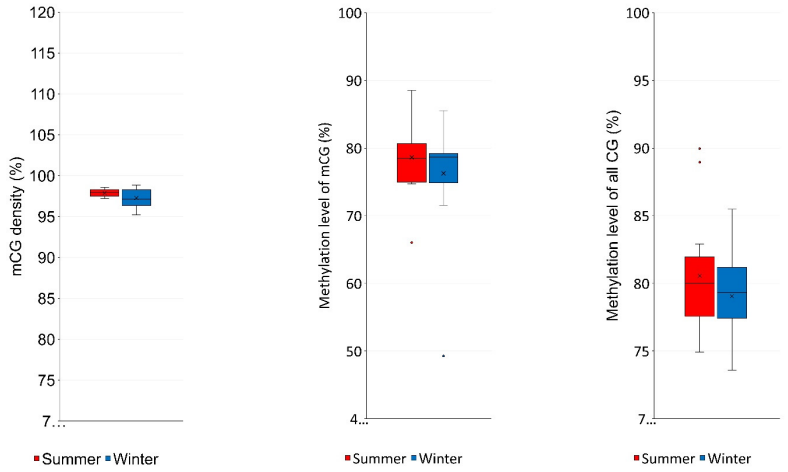

Figure S4. Comparison of DNA methylation in CG context in inactive (winter) and active (summer) periods, Related to Figure 3.

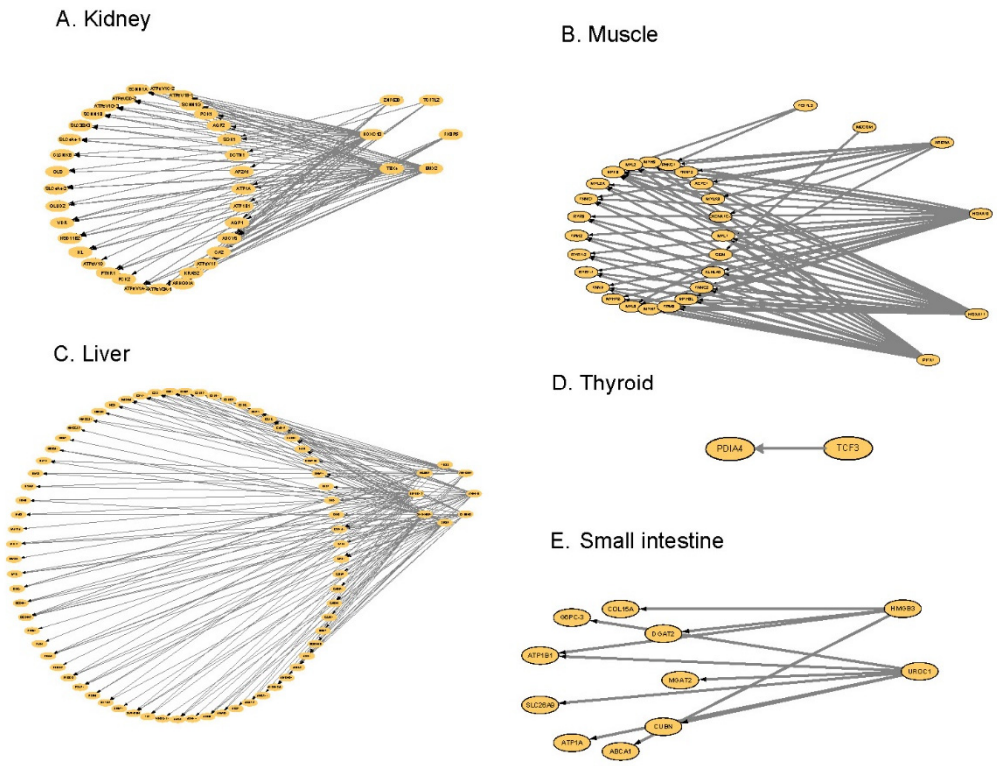

Figure S5. Associations between transcription factors (TFs) and key functional genes in each tissue, Related to Figure 5.

SUPPLEMENTARY TABLES

Table S1. Sample names for bisulfite sequencing, mRNA sequencing, and small RNA sequencing, Related to Figure 1.

	mRNA sequencing				Bisulfte sequencing		Small RNA sequencing	
	Winter		Summer		Winter	Summer	Winter	Summer
	Male	Female	Male	Female	Female	Female	Female	Female
Liver	WM_LIV	WF_LIV	SM_LIV	SF_LIV	WF_LIV	SF_LIV		
Adipose	WM_ADI	WF_ADI	SM_ADI	SF_ADI	WF_ADI	SF_ADI	WF_ADI	SF_ADI
Heart	WM_HEA	WF_HEA	SM_HEA	SF_HEA	WF_HEA	SF_HEA	WF_HEA	SF_HEA
Brain	WM_BRA	WF_BRA	SM_BRA	SF_BRA	WF_BRA	SF_BRA	WF_BRA	SF_BRA
Hypothalamus	WM_SPL	WF_SPL	SM_SPL	SF_SPL	WF_HYP	SF_HYP		
Spleen		WF_HYP		SF_HYP	WF_SPL	SF_SPL		
Kidney	WM_KID	WF_KID	SM_KID	SF_KID	WF_KID	SF_KID		
Lung	WM_LUN	WF_LUN	SM_LUN	SF_LUN	WF_LUN	SF_LUN		
Skeletal muscle	WM_MUS	WF_MUS	WM_MUS	SF_MUS	WF_MUS	SF_MUS	WF_MUS	SF_MUS
Small intestine	WM_INT	WF_INT	SM_INT	SF_INT	WF_INT	SF_INT	WF_INT	SF_INT
Thyroid		WF_THY1 / WF_THY2		SF_THY1/ SF_THY2	WF_THY1	SF_THY1		

Table S3. Serum thyroid hormone concentrations, related Figure 2.

	Active (summer) period	Inactive (winter) period	Unit
T3	>10.00	0.95	nmol/L
T4	88.09	6.42	nmol/L
FT3	18.83	1.5	pmol/L
FT4	56.48	<0.30	pmol/L
TG-Ab	271.6	20.04	KIU/L
TPO-Ab	>600.00	30.96	KIU/L
TSH	<0.005	<0.005	mIU/L

Table S4. Comparison of DNA methylation in CG context in inactive (winter) and active (summer) periods, related Figure 2.

Protein ID	Protein name	Protein description	Ratio# (iTRAQ)	Ratio# (TMT)
Alsi17612	LV001	Ig lambda chain V region 4A	1.38	1.42
Alsi14324	AF1L1	Actin filament-associated protein 1-like 1	1.24	1.3
Alsi15971	FBLN3	EGF-containing fibulin-like extracellular matrix protein 1	1.35	1.43
Alsi19475	KACB	Ig kappa chain C region, B allele	1.42	1.28
Alsi05485	SRCA	Sarcalumenin	2.93	2.21
Alsi01963	FCGBP	IgGFc-binding protein	1.76	1.89
Alsi16621	CAH6	Carbonic anhydrase 6	1.72	1.48
Alsi17112	A1AT	Alpha-1-antitrypsin	0.67	0.56
Alsi10652	RABL6	Rab-like protein 6	0.65	0.75
Alsi14288	VWF	von Willebrand factor	0.73	0.56
Alsi13698	VWA7	von Willebrand factor A domain-containing protein 7	0.79	0.65
Alsi01866	A2ML1	Alpha-2-macroglobulin-like protein 1	0.69	0.66
Alsi23845	ITIH3	Inter-alpha-trypsin inhibitor heavy chain H3	0.64	0.6
Alsi23375	XPO2	Exportin-2	0.53	0.78
Alsi12372	MCF2L	Guanine nucleotide exchange factor DBS	0.53	0.56
Alsi26905	KPYM	Pyruvate kinase PKM	0.28	0.34
Alsi02255	KPYR	Pyruvate kinase PKLR	0.56	0.64
Alsi20997	CLC11	C-type lectin domain family 11 member A	0.73	0.74
Alsi17022	RET4	Retinol-binding protein 4	0.51	0.63
Alsi04866	COMP	Cartilage oligomeric matrix protein	0.65	0.51
Alsi09977	LEG4	Beta-galactoside-binding lectin	0.45	0.44
Alsi21045	APOH	Beta-2-glycoprotein 1	0.47	0.39
Alsi01416	ACT5	Actin, cytoplasmic type 5	0.64	0.79
Alsi12373	FA10	Coagulation factor X	0.51	0.56

Winter/Summer

SUPPLEMENTARY TEXT

Data summary

We collected tissues from adult Chinese alligators in winter and summer and used multiple omics technologies (mRNA-Seq, BS-Seq, sRNA-Seq, iTRAQ, and TMT) (Figure 1, Table S1) to comprehensively explore the molecular mechanisms underlying reptile hibernation.

We produced 42 strand-specific mRNA-seq libraries, and generated 2,439 million paired-end reads, 88.36% of which were uniquely mapped to the Chinese alligator reference genome. Using these new transcriptome data as well as transcriptome data of Chinese alligator embryo (Lin et al., 2018), we annotated 27,500 protein-coding genes in the Chinese alligator genome.

Using tissues from female alligators, we produced 22 BS-seq libraries and generated 6,975 million clean read pairs (1,609 Gb of clean data), with an average depth of 16.11 per strand for each sample, and an average of 85.97% of genomic cytosines (Cs) being covered by at least five unique reads in each sample.

For sRNAs, we generated 129 million clean single-end reads from 10 sRNA-Seq libraries. 89.34% of the reads were 18–35 nt in length and were successfully mapped to the genome. We excluded other RNA species (rRNAs, tRNAs, snRNAs, snoRNAs), repetitive sequences, and transcript sequences, and with the aid of data from eight other tissues (testes and ovaries), we annotated 950 mature miRNAs. Among them, 132 miRNAs from 77 families were found in at least one other species and were thus identified as conserved miRNAs.

EXPERIMENTAL PROCEDURES

Sample sources and DNA and RNA extraction

Chinese alligator tissues (including liver, adipose, cardiac muscle, skeletal muscle, brain, hypothalamus, spleen, kidney, lung, small intestine, and thyroid tissues) were provided by the Changxing Yinjiabian Chinese Alligator Nature Reserve (CCANR) (Figure 1, Table S1). Winter samples were collected from two adult hibernating individuals (one male and one female) in January 2015, and summer samples were collected from two different adult individuals (one male and one female) during the breeding season, in May 2015. Serum samples for iTRAQ and TMT were collected from three female individuals in winter and summer, respectively. All samples were immediately stored in liquid nitrogen until use. Sample collection was performed with permission from the State Forestry Administration of China [Forest Conservation Permission Document (2014) 1545] and the Animal Ethics Committee of Zhejiang University (ZJU2015-154-13).

The gDNA used for BS-Seq and RNA used for mRNA-Seq was isolated from tissue samples using an AllPrep DNA/RNA Mini Kit (Qiagen, Hilden, Germany), according to the manufacturer's instructions. Total RNA for sRNA-Seq was isolated using a TRIzol RNA isolation kit (Invitrogen, Waltham, MA, USA) according to the manufacturer's instructions.

Strand-specific cDNA library construction and sequencing

Three micrograms of RNA was used for strand-specific cDNA library construction using a NEBNext® Ultra™ Directional RNA Library Prep Kit for Illumina® (New England Biolabs, Ipswich, MA, USA), according to the manufacturer's instructions. Library quality was evaluated on a Bioanalyzer 2100 system (Agilent Technologies, Santa Clara, CA, USA). The index-coded samples were clustered using a TruSeq PE Cluster Kit v3-cBot-HS on a cBot Cluster Generation System (Illumina Inc., San Diego, CA, USA). The library was sequenced on the Illumina HiSeq 2500 platform, generating 125-bp paired-end reads. In-house Perl scripts were used to preprocess the raw reads in fastq format. Reads containing adapter or poly-N sequences, and low-quality reads were filtered out. The Q20, Q30, and GC content of the remaining reads were calculated, and all subsequent analyses were based on these clean reads.

BS-Seq library construction and sequencing

An unmethylated λ DNA fragment was added to the gDNA to evaluate the bisulfite conversion efficiency for quality control of the bisulfite treatment. Six micrograms of gDNA and 30 ng λ DNA were mixed and fragmented into 200–300 bp by sonication. After end repair and acetylation, barcodes with methylated cytosines were added to the fragmented DNA. DNA bisulfite conversion was carried out twice using an EZ DNA methylation-GoldTM Kit (Zymo Research, Irvine, CA, USA). The DNA fragments were then amplified by PCR with KAPA Hifi HotStart Uracil + ReadyMix (Kapa Biosystems, Wilmington, MA, USA). DNA concentrations in the BS libraries were determined with a Qubit® 2.0 Fluorometer (Thermo Fisher Scientific, Waltham, MA, USA), and insert sizes were evaluated using the Bioanalyzer 2100 system. The index-coded samples were clustered using the TruSeq PE Cluster Kit v3-cBot-HS on the cBot Cluster Generation System, according to the manufacturer's instructions. The BS library was sequenced on the Illumina HiSeq 2500 platform, generating 125-bp paired-end reads. In-house Perl scripts were used to preprocess the raw reads in fastq format. Low-quality reads, reads containing adapter and poly-N sequences, and reads shorter than 36 nt following adapter removal were filtered out. The Q20, Q30, and GC content of the remaining reads were calculated, and all subsequent analyses were based on these clean reads.

Small RNA library construction and sequencing

Three micrograms of total RNA was used to construct sRNA libraries using a NEBNext® Multiplex Small RNA Library Prep Set for Illumina® (New England Biolabs), according to the manufacturer's instructions. The Agilent Bioanalyzer 2100 system was used for library quality assessment. The index-coded samples were clustered using the TruSeq SR Cluster Kit v3-cBot-HS on the cBot Cluster Generation System. After cluster generation, the sRNA libraries were sequenced on an Illumina HiSeq 2500 platform, generating 50-bp single-end reads.

RNA-Seq data analysis

The new transcriptome data produced in this study as well as transcriptome data of Chinese alligator embryo (Lin et al., 2018) were used to identify genes in Chinese alligator genome. An index of the Chinese alligator reference genome was built using Bowtie2 (Langmead and Salzberg, 2012),

and the cleaned reads were mapped to the reference genome using TopHat v. 2.0.12 (Kim et al., 2013). All aligned reads were assembled, and Cufflinks v. 2.1.1 was used to identify genes (Trapnell et al., 2010). TransDecoder and CPC were used to identify the coding region and protein-coding potential of each novel transcript (Haas et al., 2013; Kong et al., 2007). Genes with open reading frames larger than 150 bp and high protein-coding potential (score > 0) were subjected to further analysis. Transcription factor genes were identified by aligning all 27,500 genes to the animal transcription factor database TFDB2.0 (Zhang et al., 2015), using hmmsearch (Eddy, 2011).

Reads mapped to each gene were counted using HTSeq v. 0.6.1 (Anders et al., 2015), and differential gene expression between each pair of samples was analyzed using the DEGseq R package v. 1.12.0 (Mortazavi et al., 2008). Genes with an FDR < 0.005 and |log2(fold change)| > 1 were considered differentially expressed genes (DEGs). To correspond this with BS-Seq and sRNA-Seq data, we focused on the different season-biased transcriptomes of the female alligator for most of our analyses. However, we noted that gene expression patterns were largely similar in male and female non-gonadal tissues. The number of fragments per kilobase of exon per million mapped fragments (FPKM) was calculated to estimate gene expression levels. The WGCNA R package (Langfelder and Horvath, 2008) was used for weighted gene co-expression network analysis based the RNA-Seq data to analyze correlations in expression patterns among Chinese alligator genes. Gene expression level heatmaps were constructed using TBtools (Chen et al., 2018).

BS-Seq data analysis

BS-Seq reads were aligned to the Chinese alligator reference genome using Bismark (v. 0.12.5) with default parameters (Krueger and Andrews, 2011). The Chinese alligator reference genome was transformed into fully BS-converted versions termed “T genome” (C-to-T converted) and “A genome” (G-to-A converted) and then indexed using Bowtie2 (Langmead and Salzberg, 2012). All cytosines of the BS-converted reads were transformed to thymines, and the reads were aligned to the “T genome.” All guanines of the BS-converted reads were transformed to adenosines and the reads were aligned to the “A genome.” The sequence reads that produced a unique best alignment from the two alignments (original Watson and Crick strand) were re-aligned to the original reference genome to infer the methylation state of all cytosines in sequence reads. Multiple reads mapped to

the same regions of genome were defined as clonal duplicates and were filtered out to avoid inaccuracy that might be caused by bias during PCR amplification. The BS library conversion rate was estimated as the percentage of cytosines sequenced at cytosine positions in the λ reference genome.

To identify methylation sites, we modeled the sum of methylated cytosines (mCs) as a binomial (Bin) random variable with methylation rate (r), as mC ~ Bin (mC + umC*r).

The methylation level of each cytosine site was determined by the number of reads containing a methylated cytosine at the site of interest divided by the total number of reads covering the cytosine site. The methylation level of a specific region was calculated as the average methylation level of all cytosine sites in this region.

Differentially methylated regions (DMRs) between two samples were identified using swDMR (Wang et al., 2015). Since most of the mCs were in the CG context and the methylation levels in CHG and CHH contexts were low, we focused solely on CG sites for subsequent analyses. The sliding window was set to 1000 bp with a step length of 100 bp. To ensure statistical power, only windows with at least 10 CG sites and a coverage of 5 in each of the two compared samples were considered. Fisher's exact test was employed and only windows with an FDR-adjusted p (q) < 0.05 and greater than two-fold methylation level change were considered DMRs. Genes containing DMRs in their putative promoter or/and gene body regions were defined as differentially methylated genes (DMGs).

sRNA-Seq data analysis

sRNA reads were cleaned to eliminate unqualified reads and then mapped to the Chinese alligator genome reference sequence using Bowtie v. 2.2.3 (Langmead and Salzberg, 2012) without allowing any mismatch. We then annotated the reference genome sequence using the Rfam database (Kalvari et al., 2018) and RepeatMaker (Smit et al., 2013-2015), and reads corresponding to rRNAs, tRNAs, snRNAs, snoRNAs, and repeat sequences, as well as exons and introns were removed. miREvo v. 1.1 (Wen et al., 2012) and mirdeep2 (Friedlander et al., 2012) were used to predict miRNAs through exploration of the secondary structure, the Dicer cleavage site, and the minimum

free energy of the reads. Predicted miRNAs were subjected to Rfam (Kalvari et al., 2018) for miRNA family analysis and identification of conserved miRNAs (found in at least one other species). In-house scripts were applied to obtain miRNA counts. Finally, the expression level of each miRNA was normalized as the number of transcripts mapped to the miRNA per million transcripts (TPM). DEGseq R package was used to analyze differential miRNA expression between paired samples (Wang et al., 2010). miRNAs with $q < 0.01$ and $|\log2(\text{fold change})| > 1$ were assigned as DEmiRs. MiRanda, RNAhybrid, and PITA were used to predict target genes of miRNAs (Betel et al., 2010; Kertesz et al., 2007; Rehmsmeier et al., 2004). Target genes approved by at least one software package were considered targets. DESeq R package (Anders and Huber, 2010) was used to carry out principal component analysis (PCA) of sRNA-Seq data of the gonad samples and construct the plot.

GO and KEGG enrichment analyses

The GOseq 2.12 R package was used for GO enrichment analysis (Young et al., 2010). The KOBAS software package was employed for KEGG pathway enrichment analysis (Mao et al., 2005). GO terms and KEGG pathways with a $q < 0.05$ were regarded as significantly enriched.

TMT/iTRAQ protein quantification and data analysis

To reduce protein complexity and interference from highly abundant proteins, we used a ProteoMinerTM Kit (Bio-Rad Laboratories, Hercules, CA, USA) according to the manufacturer's instructions to deplete high- abundance proteins in the serum samples. Protein concentrations were determined by Bradford protein assay (Bio-Rad Laboratories). Total protein (100 μg) was digested with Trypsin Gold (Promega, Madison, WI, USA) using a protein/trypsin ratio of 30:1 at 37 °C for 16 h. The peptides were dried by vacuum centrifugation and reconstituted in 0.5 M triethylammonium bicarbonate buffer and processed according to the manufacturer's instruction for 8-plex iTRAQ (Applied Biosystems, Waltham, MA, USA) and 6-TMT labeling (Thermo Fisher Scientific). The labeled peptide mixtures were then pooled and dried by vacuum centrifugation. The peptides were separated by SCX chromatography using a LC-20AB HPLC Pump system (Shimadzu, Kyoto, Japan) and analyzed by LC-ESI-MS/MS analysis using a Q Exactive mass spectrometer (Thermo Fisher Scientific) coupled to the HPLC.

Peptides and proteins were identified by searching against the Chinese alligator database containing 27,500 sequences using the Mascot search engine v. 2.3.02 (Matrix Science, London, UK). Quantitative protein ratios were weighted and normalized by the median ratio in Mascot. We compared pairs of winter and summer samples. Only ratios with $p < 0.05$ and a fold change > 1.2 or < 0.83 in a least one pair were considered a significantly season-biased differentially expressed protein, and those with a different change trend in any pair were excluded.

SUPPLEMENTAL REFERENCES

Anders, S., and Huber, W. (2010). Differential expression analysis for sequence count data. Genome Biol 11, R106.

Anders, S., Pyl, P.T., and Huber, W. (2015). HTSeq--a Python framework to work with high-throughput sequencing data. Bioinformatics 31, 166-169.

Betel, D., Koppal, A., Agius, P., Sander, C., and Leslie, C. (2010). Comprehensive modeling of microRNA targets predicts functional non-conserved and non-canonical sites. Genome Biol 11, R90.

Chen, C., Xia, R., Chen, H., and He, Y. (2018). TBtools, a Toolkit for Biologists integrating various biological data handling tools with a user-friendly interface. bioRxiv, 289660.

Eddy, S.R. (2011). Accelerated Profile HMM Searches. PLoS Comput Biol 7, e1002195.

Friedlander, M.R., Mackowiak, S.D., Li, N., Chen, W., and Rajewsky, N. (2012). miRDeep2 accurately identifies known and hundreds of novel microRNA genes in seven animal clades. Nucleic Acids Res 40, 37-52.

Haas, B.J., Papanicolaou, A., Yassour, M., Grabherr, M., Blood, P.D., Bowden, J., Couger, M.B., Eccles, D., Li, B., Lieber, M., et al. (2013). De novo transcript sequence reconstruction from RNA-seq using the Trinity platform for reference generation and analysis. Nat Protoc 8, 1494-1512.

Kalvari, I., Argasinska, J., Quinones-Olvera, N., Nawrocki, E.P., Rivas, E., Eddy, S.R., Bateman, A., Finn, R.D., and Petrov, A.I. (2018). Rfam 13.0: shifting to a genome-centric resource for non-coding RNA families. Nucleic Acids Res 46, D335-D342.

Kertesz, M., Iovino, N., Unnerstall, U., Gaul, U., and Segal, E. (2007). The role of site accessibility in microRNA target recognition. Nat Genet 39, 1278-1284.

Kim, D., Pertea, G., Trapnell, C., Pimentel, H., Kelley, R., and Salzberg, S.L. (2013). TopHat2: accurate alignment of transcriptomes in the presence of insertions, deletions and gene fusions. Genome Biol 14, R36.

Kong, L., Zhang, Y., Ye, Z.Q., Liu, X.Q., Zhao, S.Q., Wei, L., and Gao, G. (2007). CPC: assess the protein-coding potential of transcripts using sequence features and support vector machine. Nucleic Acids Res 35, W345-349.

Krueger, F., and Andrews, S.R. (2011). Bismark: a flexible aligner and methylation caller for Bisulfite-Seq applications. Bioinformatics 27, 1571-1572.

Langfelder, P., and Horvath, S. (2008). WGCNA: an R package for weighted correlation network analysis. BMC Bioinformatics 9, 559.

Langmead, B., and Salzberg, S.L. (2012). Fast gapped-read alignment with Bowtie 2. Nature methods 9, 357-359.

Lin, J.Q., Zhou, Q., Yang, H.Q., Fang, L.M., Tang, K.Y., Sun, L., Wan, Q.H., Fang, S.G. (2018). Molecular mechanism of temperature-dependent sex determination and differentiation in Chinese alligator revealed by developmental transcriptome profiling. Science Bulletin, 63:209-212.

Mao, X., Cai, T., Olyarchuk, J.G., and Wei, L. (2005). Automated genome annotation and pathway identification using the KEGG Orthology (KO) as a controlled vocabulary. Bioinformatics 21, 3787-3793.

Mortazavi, A., Williams, B.A., McCue, K., Schaeffer, L., and Wold, B. (2008). Mapping and quantifying mammalian transcriptomes by RNA-Seq. Nature methods 5, 621-628.

Rehmsmeier, M., Steffen, P., Hochsmann, M., and Giegerich, R. (2004). Fast and effective prediction of microRNA/target duplexes. RNA 10, 1507-1517.

Smit, A., Hubley, R., and Green, P. (2013-2015). RepeatMasker Open-4.0.

Trapnell, C., Williams, B.A., Pertea, G., Mortazavi, A., Kwan, G., van Baren, M.J., Salzberg, S.L., Wold, B.J., and Pachter, L. (2010). Transcript assembly and quantification by RNA-Seq reveals unannotated transcripts and isoform switching during cell differentiation. Nat Biotechnol 28, 511-515.

Wang, L.K., Feng, Z.X., Wang, X., Wang, X.W., and Zhang, X.G. (2010). DEGseq: an R package for identifying differentially expressed genes from RNA-seq data. Bioinformatics 26, 136-138.

Wang, Z., Li, X., Jiang, Y., Shao, Q., Liu, Q., Chen, B., and Huang, D. (2015). swDMR: a sliding window approach to identify differentially methylated regions based on whole genome bisulfite sequencing. PLoS One 10, e0132866.

Wen, M., Shen, Y., Shi, S., and Tang, T. (2012). miREvo: an integrative microRNA evolutionary analysis platform for next-generation sequencing experiments. BMC Bioinformatics 13, 140.

Young, M.D., Wakefield, M.J., Smyth, G.K., and Oshlack, A. (2010). Gene ontology analysis for RNA-seq: accounting for selection bias. Genome Biol 11, R14.

Zhang, H.M., Liu, T., Liu, C.J., Song, S., Zhang, X., Liu, W., Jia, H., Xue, Y., and Guo, A.Y. (2015). AnimalTFDB 2.0: a resource for expression, prediction and functional study of animal transcription factors. Nucleic Acids Res 43, D76-81.